

# **Laboratory measurements of electrical conductivities of hydrous and dry Mt. Vesuvius melts under pressure**

POMMIER A.<sup>1,2</sup>, GAILLARD F.<sup>1,2</sup>, PICHAVANT M.<sup>1,2</sup>, SCAILLET B.<sup>1,2</sup>

<sup>1</sup>*Université d'Orléans, Institut des Sciences de la Terre d'Orléans, UMR 6113, 45067, Orléans, France*

<sup>2</sup>*CNRS/INSU, Institut des Sciences de la Terre d'Orléans, UMR 6113, 45071 Orléans, France*

**Abstract**

Quantitative interpretation of MT anomalies in volcanic regions requires laboratory measurements of electrical conductivities of natural magma compositions. The electrical conductivities of three lava compositions from Mt. Vesuvius (Italy) have been measured using an impedance spectrometer. Experiments were conducted on both glasses and melts between 400 and 1300°C, and both at ambient pressure in air and at high pressures (up to 400 MPa). Both dry and hydrous (up to 5.6 wt% H<sub>2</sub>O) melt compositions were investigated. A change of the conduction mechanism corresponding to the glass transition was systematically observed. The conductivity data were fitted by sample-specific Arrhenius laws on either side of T<sub>g</sub>. The electrical conductivity increases with temperature and is higher in the order tephrite, phonotephrite to phonolite. For the three compositions investigated, increasing pressure decreases the conductivity, although the effect of pressure is relatively small. The three compositions investigated have similar activation volumes ( $\Delta V=16-24$  cm<sup>3</sup>/mol). Increasing the water content of the melt increases the conductivity. Comparison of activation energies (E<sub>a</sub>) from conductivity and sodium diffusion, and use of the Nernst-Einstein relation allow sodium to be identified as the main charge carrier in our melts and presumably also in the corresponding glasses. Our data and those of previous studies highlight the correlation between the Arrhenius parameters E<sub>a</sub> and  $\sigma_0$ . A semi-empirical method allowing the determination of the electrical conductivity of natural magmatic liquids is proposed, in which the activation energy is modelled on the basis of the Anderson-Stuart model,  $\sigma_0$  being obtained from the compensation law and  $\Delta V$  fitted from our experimental data. The model enables the electrical conductivity to be calculated for the entire range of melt compositions at Mt. Vesuvius and also predicts satisfactorily the electrical response of other melt compositions. Electrical conductivity data for Mt. Vesuvius melts and magmas are slightly lower than the electrical anomaly revealed by MT studies.

## 1. Introduction

Electrical conductivity anomalies are revealed by magnetotelluric surveys in volcanic regions [Jones, 1999; *Partsch et al.*, 2000; *Hoffmann-Rothe et al.*, 2000; *Brasse et al.*, 2002; *Scarlato et al.*, 2004]. Their interpretation requires experimental data and models of electrical conductivity for natural magmas. Electrical conductivity reveals the mobility of charge carriers in the presence of a gradient in electrical potential. Therefore, this property is

extremely sensitive to chemical composition, as well as to phase assemblages and texture [Roberts and Tyburczy, 1999]. As a first step, models of electrical conductivity of silicate melts as a function of composition are needed. Gaillard [2004] presented electrical conductivity data for a silicic melt composition at different temperatures and pressures up to 400 MPa. An increase in conductivity associated with the addition of water was observed. Gaillard and Iacono Marziano [2005] demonstrated changes in electrical conductivity during crystallization of an intermediate composition magma and attributed the modifications observed to variations in the composition of the residual melt. Here, we use these approaches to provide the first measurements of electrical conductivity for the potassic series of Mt. Vesuvius (Italy).

were considered in this study. [Di Maio *et al.*, 1998; Manzella *et al.*, 2004; ] 6>20 the magnetotelluric (MT) data show evidence for a low-resistivity zone at a depth of approximately 6-8 km. Seismic studies [Zollo *et al.*, 1996; 1998; Auger *et al.*, 2001; Nunziata *et al.*, 2006] have identified a low-velocity layer at comparable depths and iver than its local environment. Such an anomalous layer, imaged both by the electromagnetic and the seismic data, may be interpreted as a magma chamber (see references above). To test this hypothesis, data on the electrical conductivity of Mt. Vesuvius magmas are required. T such data comparison between laboratory and field measurements of electrical conductivity is essential improv the interpretation of geophysical data and better defining geostructural features [Roberts and Tyburczy, 1999]. Previously, Scarlato *et al.* [2004] have used electrical conductivity measurements to assist the geophysical interpretations on the internal structure of Mt. Etna. In this study, electrical conductivity measurements are presented for tephrite to phonolite melt compositions. current database on electrical conductivity of silicate melts [Gaillard and Iacono Marziano 2005]. The main experimental parameters include temperature, pressure and the water content of the melt, the conductivity measurements being obtained both for dry and hydrous melts. A model fitting the electrical conductivity data has been established and is valid for the entire range of compositions considered in this paper. We compare our laboratory data with field measurements at Mt. Vesuvius and then discuss the likelihood of a magma storage zone.

## **2. Basic concepts of electrical conductivity and previous works**

he electrical conductivity of a material expresses the aptitude of charge carriers to diffuse in this material when an electrical potential is applied. It is a function of several

parameters such as T, P and composition [Tyburczy and Waff, 1983, 1985; Roberts and Tyburczy, 1999]. The pressure and temperature dependency of the electrical conductivity is described by an Arrhenius law:

$$\sigma = \sigma_0 \cdot \exp\left(\frac{-Ea - P \cdot \Delta V}{\mathfrak{R} \cdot T}\right) \quad (1),$$

where  $\sigma$  is the conductivity ( $\text{Ohm}^{-1} \cdot \text{m}^{-1}$ ),  $\sigma_0$  the pre-exponential factor ( $\text{Ohm}^{-1} \cdot \text{m}^{-1}$ ),  $Ea$  the activation energy (J),  $P$  the pressure (MPa),  $\Delta V$  the activation volume ( $\text{cm}^3/\text{mol}$ ),  $T$  the temperature (K) and  $\mathfrak{R}$  the universal gas constant.

For silicate glasses and melts, two different electrical conductivity regimes can be distinguished, respectively below and above  $T_g$  (the glass transition temperature, Dingwell, 1995; Angell, 2001; Bagdassarov et al., 2001). The Arrhenius law applies to silicate glasses (e.g. Caillot et al., 1994). In contrast, above  $T_g$ , a non Arrhenian behavior is sometimes observed, which can be accounted for by various formalisms, as the empirical VTF [e.g. Hess and Dingwell, 1996; Pfeiffer, 1998]:

$$\sigma = A_{VTF} \cdot \exp\left(\frac{B_{VTF}}{T - T_0}\right) \quad (2)$$

(where A, B and  $T_0$  are adjustable parameters) or the Caillot [Caillot et al., 1994] laws. In this study, an Arrhenian formalism was successfully applied above  $T_g$  for the three compositions investigated.

The electrical conductivity in amorphous silicates (glasses and melts) is essentially controlled by ionic mobility, electronic mobility being significant for specific conditions (low T) and compositions (iron-rich glasses, Barczynski and Murawski [2002]). The conductivity measured in amorphous silicates reflects the mobility of several charge carrier ions, the total conductivity being the sum of the individual conductivities [Gaillard, 2004]. In most cases, the conductivity is dominated by only one or two ionic species. Ionic conductivity is related to diffusive transport of charge carriers within the melt, as expressed by the Nernst-Einstein equation:

$$\sigma_i = \frac{D_i \cdot q_i^2 \cdot N_i}{k_B \cdot T \cdot Hr} \quad (3),$$

where  $D_i$  is the coefficient of diffusion of a ion i ( $\text{m}^2/\text{s}$ ),  $q_i$  its charge (C),  $N_i$  the concentration of i ( $\text{m}^{-3}$ ),  $k_B$  the Boltzmann constant ( $1.38 \cdot 10^{-23}$  J/K),  $T$  the absolute temperature (K) and  $Hr$  the Haven ratio.  $Hr$  expresses the mechanisms of migration of charge carriers within the melt. It generally ranges between 0.2 and 1 for amorphous silicates [Heinemann and Frischat,

1993] and is usually taken equal to 1 for rhyolitic melts [Gaillard, 2004 and references therein].

The electrical conductivity of silicate melts has been demonstrated to be pressure dependent [Tyburczy and Waff, 1983, 1985; Bagdassarov *et al.*, 2004; Gaillard, 2004], although in some studies performed on multiphase assemblages and at high pressure (>1 GPa) no influence of pressure was detected [Scarlato *et al.*, 2004; Maumus *et al.*, 2005]. Regarding the influence of water, Gaillard [2004] observed an increase in conductivity and a decrease of the activation energy with increasing water content, consistent with sodium mobility under dry and hydrous conditions. The strong decrease in the conductivity of hydrous phonolitic melts found by Satherley and Smedley [1985] is probably the consequence of a H<sub>2</sub>O loss, especially at high temperatures. Gaillard and Iacono Marziano [2005] performed experiments on multiphase (crystals+liquid) assemblages and showed the importance of residual melt composition on conductivity measurements. This point stresses the need for systematic investigations of the effect of melt composition on electrical conductivity.

### 3. Experiments

#### 3.1. Starting products

The starting materials were three natural samples from the Mt. Vesuvius eruptive activity: a phonolite (VES19) from the AD 79 (Pompei) eruption [Cioni *et al.*, 1995], a phonotephrite (VS88-65B) from the AD 472 (Pollena) eruption [Rosi and Santacroce, 1983] and a tephrite (VES9) from a 8<sup>th</sup> century eruption [Cioni, unpublished data] (Figure 1).

Both dry and hydrous glass samples prepared from the natural rocks were used for the electrical conductivity measurements. Each rock was finely crushed in an agate mortar. The powder was dried and then melted in air at 1500°C during ~1h. Quenching was performed in air and the resulting bubble-free glass was drilled to cylinders (either 5 or 8 mm OD, length between 4 and 8 mm). These dry glass cylinders were directly used in the electrical conductivity measurements. The composition of the dry glasses is given in Table 1 and shown in Figure 1. They cover the entire spectrum of differentiation observed at Mt. Vesuvius over the last 10 kyr [Ayuso *et al.*, 1998]. With progressive differentiation, i.e. from tephrite to phonolite, SiO<sub>2</sub>, Al<sub>2</sub>O<sub>3</sub>, Na<sub>2</sub>O and K<sub>2</sub>O increase while FeO, MgO and CaO decrease. The dry glasses have NBO/T ratios (number of non-bridging oxygens divided by number of tetrahedral cations), calculated considering all Fe as FeO and neglecting the presence of Ti [Mysen and Richet, 2005], decreasing from 0.73 (tephrite), 0.46 (phonotephrite) to 0.11

(phonolite), i.e. become more polymerised with progressive differentiation. Because of the presence of appreciable halogen concentrations in the phonolite (Table 1), the calculated NBO/T value should be considered as a minimum.

The hydrous glasses were synthesised by hydrating cylinders (either 5 or 10 mm OD) of dry glasses at high pressure. The glass cylinders were loaded into either Pt or Au capsules together with a known amount of water. The capsules were sealed by arc-welding. The hydration experiments were performed at 1250°C and 200MPa (VES19+~1 wt%H<sub>2</sub>O; VS88-65B+~3.5 wt%H<sub>2</sub>O) and at 1050°C and 300MPa (VES19+~6 wt%H<sub>2</sub>O). For each concentration of water, the duration of the hydration experiment was determined from the diffusivity of water [Watson, 1994], and lasted from 3h to more than 20h, depending on the water content and the geometry of our glass cylinders [Crank, 1975]. The hydration experiments yielded hydrous glass samples with 1.1 wt%H<sub>2</sub>O (VES19), 3.5 wt%H<sub>2</sub>O (VS88-65B) and 5.6 wt%H<sub>2</sub>O (VES19), as determined by Karl Fischer Titration. No hydrous glass sample is available for the tephrite (VES9). The hydrous glass samples, which are all bubble-free at a micrometer scale, were drilled to cylinders (5 mm OD, length between 4 and 8 mm), which were then loaded into the conductivity cell.

### **3.2. Experimental equipment and procedures**

Conductivity measurements at ambient pressure were conducted in a vertical furnace. All experiments were performed in air. Temperature, monitored with a *Eurotherm* controller, was measured by a type-S thermocouple, placed adjacent to the conductivity cell, and is known to within +/- 2°C. Both the conductivity cell and the thermocouple were located in the 3 cm hot spot of the furnace.

Experiments at high pressures (both hydration and conductivity experiments) were performed in an internally heated pressure vessel (IHPV), working vertically with argon as the pressure medium [Di Carlo *et al.*, 2006]. Total pressure was measured by a transducer and is known to within +/- 2 MPa. A double winding Mo furnace was used. Temperature was monitored with a *Eurotherm* controller and recorded by two thermocouples adjacent to the sample (thermal gradient <5°C). Although the fO<sub>2</sub> in the IHPV experiments is not precisely known, the use of pure argon (i.e. H-free atmosphere) as pressure medium maintained relatively oxidizing redox conditions [Gaillard, 2004; Di Carlo *et al.*, 2006], even if less oxidizing than in the ambient pressure experiments performed in air.

### 3.3. Analytical techniques

A SEM (JEOL WINSET JSM 6400, Polytech'Orléans-ISTO) was systematically used in back-scattered mode (1) to investigate processes at the interfaces between the sample and the conductivity cell and (2) to detect the presence of crystals in auxiliary experiments performed to define the crystallisation interval of the three samples at 1 bar.

A Camebax SX-50 electron microprobe (BRGM-CNRS-Université d'Orléans, Orléans) was used to analyse (1) the starting glasses, (2) the experimental products (glasses and crystals) after the conductivity measurements and (3) the components of the conductivity cell (electrodes and alumina ceramic parts, Figure 3) after the conductivity measurements. Analyses were conducted at 15 kV, 6 nA, 10 s on peak and 5 s on background. A defocused beam (8-10  $\mu\text{m}$ ) was used to analyse glasses whereas a focused (1-2  $\mu\text{m}$ ) beam was used to analyse crystals.

The water content of hydrous samples was measured by Karl Fischer Titration (KFT) at ISTO, Orléans [Westrich, 1987; Behrens *et al.*, 1996]. Glass samples of at least 10mg were analysed to ensure reproducibility and accuracy. Duplicate analyses were performed and the results averaged (Table 2). To check the homogeneity of water, the starting glasses were analysed by FTIR using a Nicolet Magna 760 instrument attached to a Nic-Plan microscope [Gaillard *et al.*, 2001]. A Globar SiC source, a MTC/A detector and a  $\text{CaF}_2$  beamsplitter were used. Spectra were collected over the 2000-7400  $\text{cm}^{-1}$  range with a 4 or 8  $\text{cm}^{-1}$  resolution and accumulated during 128 scans on double polished samples prepared from each glass. Water concentrations calculated from various analytical spots were identical, showing that water is distributed homogeneously.

### 3.4. Conductivity measurements

#### 3.4.1. Conductivity cell and electrical measurements

For all experiments, we adopted a two-electrode configuration [e.g. Bagdassarov *et al.*, 2001], with the electrical impedance being radially measured. The inner electrode (a 1 mm Pt wire) was inserted in the centre of previously drilled glass cylinders. A Pt tube surrounding the sample (OD: 5 mm, thickness: 0.2 mm) served as the external electrode. Two distinct configurations were retained for the conductivity cell. The 0.1 MPa measurements used an open cell with the inner electrode inserted from the top (Figure 2a) and the high pressure a closed cell with the inner electrode inserted from the bottom (Figure 2b). For the 0.1 MPa experiments, the conductivity cell is terminated at its bottom by a drilled alumina

plug, while the top is in direct contact with air (Figure 2a). For the high pressure experiments, the Pt tube is circle-welded at its basis on a Pt cap and separated from the glass sample by an alumina disk. The other extremity of the conductivity cell consists of a drilled alumina plug (Figure 2b). For both configurations, the alumina plug is glued onto the Pt tube by using a low thermal expansion inorganic cement (Ceramabond). The stability of the cell geometry is essentially ensured by the Pt tube and the alumina plug. Examination of the cell after the experiments confirmed that the initial geometry was conserved. Some melt migration along the walls of the Pt tube was observed in the 0.1 MPa experiments but its influence on geometry is negligible [Gaillard, 2004]. Sometimes the low-viscosity tephritic melt flowed through the drilled alumina plug, in which case results were discarded and the experiment repeated. The experiment was also repeated when a gas bubble grew in the glass cylinder, as observed from inspection of the conductivity cell. Note that with the cell geometries described in Figure 3, alumina and the inorganic cement may potentially contribute to the measured conductivity, in addition to the silicate sample. However, 0.1 MPa measurements of the conductivity of the inorganic cement showed that its influence is negligible, and Gaillard [2004] and Gaillard and Iacono Marziano [2005] have shown that the influence of alumina can also be neglected. Therefore, the silicate sample is the unique conductive path of the used cell assembly.

In this study, electrical conductivities were derived from complex impedance spectroscopy [Roberts and Tyburczy, 1994]. Electrical impedances of samples were determined at variable frequencies using a Solartron 1260 Impedance Gain Phase Analyser, (Schlumberger Co.), equipped with Zview software package [Huebner and Dillenburg, 1995; Gaillard, 2004; Maumus et al., 2005]. For each measurement, frequencies were scanned from 1 Hz to  $10^6$  Hz. Perturbations on electric signals were reduced by minimizing the length of coaxial cables between the impedance spectrometer and the sample. At 0.1 MPa, electrical measurements were performed along heating cycles from  $\sim 400^\circ\text{C}$  to  $\sim 1300^\circ\text{C}$ , i.e. the electrical conductivities of glass and liquid were measured sequentially. At high pressures, electrical conductivities of glass were measured first by keeping temperatures below  $T_g$ , while pressure was varied. Then, temperature was increased so as to reach the stable liquid region and electrical conductivities were recorded at different pressures. In order to demonstrate reproducibility, electrical results obtained along heating cycles were checked against measurements at selected temperatures along cooling cycles. We also checked our experimental setup by comparing the electrical conductivity of a borosilicate with data

obtained using the procedure of *Malki and Echehut* [2003] (Malki, personal communication, 2007), which uses geometries different from this study. No noticeable differences in electrical conductivity values were noticed for this composition between 300 and 900°C, which lends confidence to the validity of our method, particularly for the calculation of the geometric factor.

Although this paper is aimed at the presentation of electrical conductivity data for glasses and liquids, partial crystallisation of the samples was occasionally observed. Additional quenching experiments were performed on each sample to delineate the crystallisation intervals at 0.1 MPa, identified in the T range [ $\geq 800^\circ\text{C}$ -liquidus (depending on the composition, see Table 2)]; the crystallisation is heterogeneous, mainly occurring on the walls of the Pt electrodes and is essentially out of equilibrium. This process was heavily marked for the tephritic and phonotephritic samples, whereas the phonolite VES19 weakly crystallised. The interpretation of the conductivity values in terms of liquid and crystals contributions was not possible since the amount of crystals in the conductivity cell could not be characterised. Therefore, electrical conductivity data acquired in the crystallisation range are neither presented (except for VES19 at 0.1 MPa, see 4.2.) nor considered in the interpretations below.

#### 3.4.2. Data reduction

The electrical response of the sample to a scan in frequency is directly observed in the Nyquist plan ( $Z'$ ,  $Z''$ ), since the complex impedance can be written as the sum of a real and an imaginary parts,  $Z' + jZ''$ , with  $j^2 = -1$  (Figure 3). As previously underlined, [e.g. *Huebner and Dillenburg*, 1995], the first part of the response (semi-circle, for  $Z' < R$ , where R is the electrical resistance of the sample) represents the electrical response of the sample, whereas the second part, (mostly linear, for  $Z' > R$ ), represents the effect of the interface between the sample and the electrode. The whole measured response can be modelled by a RC-CPE circuit [*Huebner and Dillenburg*, 1995] (Figure 3).

The shape of impedance spectra changed with temperature: at low temperatures (below  $\sim 750^\circ\text{C}$ ) an impedance arc was observed in the high frequency part; at higher temperatures, no impedance was recorded. However, the quasi-linear portion in the low frequency range was observed in both temperature domains and its intersection with the real axis yielded the value of the resistance of the sample (Figure 3).

For given T and P conditions, electrical measurements were repeated until a stable value of R was reached (generally rapidly within a few minutes, Figure 4a). In the case of experiments that partially crystallised during the heating cycle, attainment of the stable liquid region required dissolution of all pre-existing crystals. Crystal dissolution is marked by a progressive increase in electrical conductivity and, to be completed, needed durations of the order of a few hours (Figure 4b).

The electrical conductivity  $\sigma$  is obtained from the electrical resistance R of the sample by using the relation [e.g. *Gaillard, 2004*]:

$$\sigma = \frac{1}{G.R} \quad (4)$$

$$\text{where } G = \frac{2\pi L}{\ln\left[\frac{d_{ext}}{d_{int}}\right]} \quad (5)$$

G is the geometric factor (from  $\sim 1.4$  to  $1.8 \cdot 10^{-2}$  m), L the length of the sample (m), and  $d_{ext}$  and  $d_{int}$  are respectively the external and internal diameters of the glass cylinder (m). In this study, L,  $d_{ext}$  and  $d_{int}$  are assumed to be constant, since the geometry of the conductivity cell is essentially conserved during the experiments. Error propagation of typical uncertainties on L,  $d_{ext}$ ,  $d_{int}$  and R (at low temperatures, R is known to +/- 5 Ohm and, at high temperatures, to +/- 0.5 Ohm) shows that the uncertainty on  $\sigma$  is in the range 3.6-8%, except for VES19 at high temperatures (1200-1300°C): 8-10.3%.

## 4. Results

### 4.1. Interaction processes between conductivity cell and sample

In order to characterize chemical interaction processes between components of the conductivity cell and sample that could affect the measurements, the interfaces between glass and Pt electrodes and glass and alumina have been carefully investigated after most electrical conductivity experiments.

Electron microprobe traverses performed across the Pt electrode – glass interfaces showed no significant variations in oxide concentrations, except for FeO. Interface FeO concentrations were depleted by  $\sim 10\%$  in the high-pressure experiment performed on VES9, but showed significant change neither in the case of the 1 atm experiment on VES9 nor of the high-pressure experiment on VS88-65B (Table 2). Iron was found to be present at very low concentrations ( $< 0.5\%$ ) in Pt electrodes from the 0.1 MPa experiments. However, in the high-pressure experiments, iron concentrations at the wt% level were sometimes detected in the

outer rims of the Pt electrodes, consistent with more reducing conditions than at 0.1 MPa. Therefore, we conclude that iron loss to the electrodes was of minor importance in this study. Electron microprobe traverses across the Al<sub>2</sub>O<sub>3</sub> plug – glass interface revealed the presence near the alumina plug of an Al-, K-, Na-enriched and Si-, Fe-, Mg-depleted glass zone. However, these chemically anomalous zones are about 200-300 μm thick, represent only ~3% of the total height of the sample, and their presence was neglected in the interpretation of the results.

At the interface between the glass sample and alumina, a nearly continuous 10-25 μm thick layer of Al-Mg-Fe-spinel was observed for the phonotephritic and tephritic compositions. For the phonolitic composition, no spinel was observed and the interface is crystal-free. Because the electrical conductivity of Fe-Al-Mg spinel is known [Nell *et al.*, 1989], the contribution of the spinel and melt to the measured conductivity can be evaluated. Since the spinel and liquid arrangement corresponds to a parallel model, the measured electrical resistance (effective resistance) of the circuit can be written as follow [after Glover *et al.*, 2000]:

$$\frac{1}{R_{eff}} = \frac{\chi_{sp}}{R_{sp}} + \frac{(1 - \chi_{sp})}{R_{liq}} \quad (6)$$

where R<sub>eff</sub> is the effective resistance (Ohm),  $\chi_{sp}$  the volume fraction of spinel, R<sub>sp</sub> the resistance of the spinel (Ohm) and R<sub>liq</sub> the resistance of the studied sample (Ohm). The calculations show that, in the case of the phonotephritic melt, the measured conductivity corresponds to at least 99.998% of the conductivity of the melt and, in the case of the tephritic melt, to at least 99.500%. Thus, because the volume of spinel is much lower than the volume of the melt, the melt is the dominant electrical contributor.

#### 4.2. Effect of temperature and melt composition

For the three samples investigated, electrical conductivity data are available in two distinct temperature domains, separated by an interval where crystallisation was observed. In both domains, increasing T increases the electrical conductivity (Figure 5). Good agreement is observed between data obtained along heating cycles and the few data points obtained along cooling cycles, which demonstrates reproducibility. The non-linearity between log  $\sigma$  and 10<sup>4</sup>/T over the whole interval of temperature indicates a change of the conduction mechanism. Such a change in behavior, graphically represented by a kink in the conductivity data versus T plot (Figure 5), is classically interpreted as corresponding to the glass transition temperature

( $T_g$ ) [Dingwell, 1995; Angell, 2001; Bagdassarov *et al.*, 2001]. It marks the transition between an activated ( $T < T_g$ ) and an assisted ( $T > T_g$ ) transport mechanism [Déportes *et al.*, 1994]. On Figure 5,  $T_g$  is located at  $\sim 670^\circ\text{C}$  ( $\pm 15^\circ\text{C}$ ) for the three compositions studied. For the three samples, the increase in electrical conductivity between 450 and  $1300^\circ\text{C}$  is of about 4.5 log units for the tephrite and the phonotephrite, and 4 log units for the phonolite. At temperatures below  $T_g$ , the conductivity displays a linear increase with reciprocal temperature and the data can be fitted by sample-specific Arrhenius laws (Table 3). Above  $T_g$ , an empirical VTF formalism was first considered to fit the data. However, a low value of  $T_0$  (the VTF temperature) was obtained, and the data in the liquid region were better fitted by sample-specific Arrhenius laws (Table 3). The use of  $\sigma_0/T$  instead of  $\sigma_0$  in the Arrhenian formalism was also considered but did not improve the fit. In both glass and melt regions,  $\sigma_{\text{phonolite}} > \sigma_{\text{phonotephrite}} > \sigma_{\text{tephrite}}$  so that the more polymerised the melt, the higher the conductivity. At  $1200^\circ\text{C}$ , the conductivity of the phonolite, the most polymerised sample, is 0.6 log unit higher than the conductivity of the tephrite, the less polymerised sample.

### 4.3. Effect of pressure

As shown on Figure 6, increasing  $P$  decreases the conductivity. This effect was observed for the three compositions, both in the glass and liquid regions. The variation of electrical conductivity with pressure is between 0.5 and 0.25 log units in the glass and liquid regions, respectively, between 0.1 and 400 MPa. For example, at  $1200^\circ\text{C}$ , the electrical conductivity of the tephrite at 400 MPa decreases by  $\sim 50\%$  relative to that at 0.1 MPa. These variations are in the same range than those observed by Tyburczy and Waff [1983] for tholeiitic-andesitic melts. Thus, our results confirm that the electrical conductivity is less dependent on pressure than on temperature [Tyburczy and Waff, 1983].

In detail, the decrease in conductivity with increasing pressure is more marked in the liquid than in the glass region and appears to vary with the nature of the starting sample (Fig 6b). The pressure effect is the smallest for the tephrite composition, whilst the phonotephrite and phonolite samples exhibit similar pressure dependences. This is consistent with the influence of pressure being related to the degree of melt polymerisation, the more polymerised the melt, the greater the pressure dependency of the electrical conductivity [Tyburczy and Waff, 1983]. Nevertheless, the compositional influence on the effect of pressure remains small, as illustrated by the similar  $\Delta V$  values of the Arrhenius laws obtained for the three compositions ( $16\text{-}24\text{ cm}^3/\text{mol}$ , Table 3).

#### 4.4. Effect of water

Conductivity data for hydrous phonotephrite and phonolite melts under pressure show that increasing the water content of the melt increases the conductivity (Figure 7). The influence of H<sub>2</sub>O is more marked at low than at high temperature. In the Log  $\sigma$  vs 1/T plot, the slope of the Arrhenius equation flattens with increasing melt water concentration. This corresponds to a progressive decrease of E<sub>a</sub> from 93 kJ/mol (dry), 68 kJ/mol (1.1 wt%H<sub>2</sub>O) to 61 kJ/mol (5.6 wt%H<sub>2</sub>O) for the phonolite sample (Table 3). This lowering of E<sub>a</sub> due to water is consistent with the results of *Watson* [1994] for water diffusion and the results of *Gaillard* [2004] for electrical conductivity in more polymerised melts (rhyolite). At 1250°C, the increase in electrical conductivity per wt% of dissolved H<sub>2</sub>O is about 0.1-0.2 log units with little difference between the two samples (Figure 7b).

Analysis of the glasses after the conductivity measurements shows that all hydrous samples are partially crystallised and have lost water to different extents (Table 2). Crystallisation in those samples is most probably related to the slow quenches that were applied after the completion of the electrical measurements. The loss of water probably occurs near the end of the experiment since (1) a regular and progressive increase of the electrical conductivity is observed with increasing melt water content and (2) the effect of water on conductivity is clearly marked on the whole T range. For the two heating cycles performed on hydrous phonolite liquids (Figure 7a), an influence of water is apparent until the highest temperatures investigated (1250 and 1276°C, Table 2), suggesting that the bulk of the water was still dissolved in the melts.

## 5. Discussion

### 5.1. Transport mechanisms

The evolution of the electrical conductivity with temperature demonstrates a dual behavior below and above the glass transition (Figure 5). For the three samples studied, two different Arrhenius laws (Table 3) are necessary to model the temperature and pressure dependence of the electrical conductivity, underlining the existence of two different transport mechanisms (conductivity regimes) within the studied samples (i.e. one in the glass region, the other in the liquid region) [*Dingwell*, 1995]. A similar value of T<sub>g</sub> was observed for the three dry studied compositions (~670°C (+/-15°C), in agreement with the value obtained for a phonolite by *Giordano et al.* [2005]). Our conductivity measurements did not permit to

determine a significant effect of pressure on T<sub>g</sub> values. Previous work [*Bagdassarov et al.*, 2004] has shown only a small increase of T<sub>g</sub> with pressure (a few °C/GPa).

Our determined values of activation volumes range between 16 and 24 cm<sup>3</sup>/mol. These are comparable to those obtained by *Gaillard* [2004] on a rhyolite (20 cm<sup>3</sup>/mol) and by *Tyburczy and Waff* [1985] on an andesite (17.9 cm<sup>3</sup>/mol) at similar pressures (<1 GPa). However, at pressures >1 GPa, ΔV values are generally much lower (<6 cm<sup>3</sup>/mol) than at lower pressures [*Tyburczy and Waff*, 1985]. This range of activation volumes is consistent with ΔV=5.4 cm<sup>3</sup>/mol for an albite melt between 2.6 and 5.3 GPa [*Bagdassarov et al.*, 2004]. We conclude that our determined ΔV are similar to those derived from other studies at relatively low pressures.

Activation energies (E<sub>a</sub>) from conductivity data [this study, *Presnall*, 1972; *Tyburczy and Waff*, 1983, 1985; *Park and Ducea*, 2003; *Scarlato et al.*, 2004; *Gaillard*, 2004; *Gaillard and Iacono Marziano*, 2005] can be compared with activation energies of diffusion data on sodium [*Henderson et al.*, 1985; *Jambon*, 1982] in Figure 8a. The sodium was indeed identified as the main charge carrier in silicic to basaltic melts [*Tyburczy and Waff*, 1983, 1985; *Gaillard*, 2004; *Gaillard and Iacono Marziano*, 2005]. Globally, E<sub>a</sub> increases as NBO/T increases. Apart from the diffusion data for the Pitchstone rhyolite that shows an anomalously high E<sub>a</sub> [*Henderson et al.*, 1985], there is good agreement between E<sub>a</sub> derived from Na-diffusion and electrical conductivity. This allows us to interpret sodium as the dominant charge carrier in the liquid region of our studied samples.

On Figure 8b, pre-exponential factors σ<sub>0</sub> are plotted versus activation energies E<sub>a</sub> for both Na-diffusion and conductivity measured in compositions including basalt-andesite-phonolite-rhyolite. All data consistently plot on a single linear trend, which enlightens the influence of composition on Arrhenius parameters. The data of studies mentioned above, for conductivity measurements and for Na-diffusion measurements, are plotted. The data point of *Presnall et al.* [1972] suggests that the conductivity is also probably dominated by sodium in their synthetic basaltic melt. The dataset can be successfully fitted by a single trend, which is illustrated by the straight line on Figure 8b:

$$E_a = 12.5 \ln \sigma_0 - 9.9 \quad (7)$$

where E<sub>a</sub> is the electrical activation energy (kJ/mol) and σ<sub>0</sub> is the pre-exponential factor ((Ohm.m)<sup>-1</sup>). Such a correlation between Arrhenius parameters is often mentioned in the literature as the compensation effect [*Wu and Zheng*, 2003]. Combination of Eq. 7 and Eq. 1 implies that all the conductivity data converge to a unique value at a given temperature, T<sub>char</sub>,

called the characteristic temperature, according to *Wu and Zheng* [2003]. We obtained a value of  $T_{\text{char}}$  of  $\sim 1290^{\circ}\text{C}$ , corresponding to a conductivity of  $\sim 3.16 \text{ (Ohm.m)}^{-1}$ . An increase of the value of  $E_a$  together with  $\sigma_0$  is observed along with a decrease of the degree of polymerisation of the melt: the right part of the diagram ( $\text{Ln } \sigma_0 > 9$ ) is characterised by high values of  $E_a$  and corresponds to tholeiitic, basaltic to tephritic melts, whereas in the left part ( $\text{Ln } \sigma_0 < 9$ ) rhyolitic, andesitic to phonolitic melts present low values of  $E_a$ .

The nature of the main charge carriers in the liquid region, irrespective of the melt composition and the water content of the melt, is confirmed using the Nernst-Einstein equation (3), which shows that the alkali, particularly sodium, contribute to more than 80% of the total electrical conductivity. Calculation was performed at  $1300^{\circ}\text{C}$  with diffusivity data from *Alibert et al.*, 1980; *Henderson et al.*, 1985; *Wendlandt*, 1991; *Kress et al.*, 1993. The electrical conductivity contribution of each potential charge carrier ( $\sigma_i$ ,  $i$  being the ion charge carrier :  $\text{Na}^+$ ,  $\text{K}^+$ ,  $\text{Ca}^{2+}$ ,  $\text{Mg}^{2+}$ ,  $\text{Al}^{3+}$ ,  $\text{Si}^{4+}$  and also  $\text{O}^{2-}$ ) was calculated. The Haven ratio  $H_r$  was taken equal to 1 [*Gaillard*, 2004], which is equivalent to assume that the charge carriers move independently through a direct interstitial mechanism [*Heinemann and Frischat*, 1993; *Roling*, 1999]. Attempts to calculate  $H_r$  directly from Eq.3 using measured electrical conductivities and diffusivities from the literature yielded poorly constrained results because there are no Na diffusion data available for our studied compositions. Nevertheless, a value of  $H_r$  of 0.38 is obtained for our tephritic melt by using the diffusion coefficient for  $\text{Na}^+$  in basaltic melt from *Henderson et al.* [1985]. We note that *Gaillard and Iacono Marziano* [2005] calculated a Haven ratio of 0.4 for their basaltic composition, which compares well with our estimation and suggests that depolymerised silicate melts tend to yield lower  $H_r$  values than polymerized ones.

For all compositions shown in Figure 8, at  $T < T_{\text{char}}$ , the more polymerised the melt, the greater the conductivity, i.e. charge carriers migrate faster in polymerised melts than in depolymerised melts. This is in agreement with the data of *Henderson et al.* [1985] and *Mungall* [2002] who stressed out that the diffusion of alkali in silicate melts increases with the degree of polymerisation. In the same way, the more polymerised the melt, the greater the viscosity. Thus, both the electrical conductivity and the viscosity react in the same direction to changes in the degree of polymerisation. Note that this is in apparent contradiction with Eyring's law, which specifies that the diffusion coefficient (or the electrical conductivity) would be inversely proportional to the viscosity [*Reid et al.*, 2001]:

$$D = \frac{k_B T}{\eta \lambda} \quad (8)$$

where  $D$  is the diffusion coefficient ( $\text{m}^2/\text{s}$ ),  $k_B$  the Boltzmann constant,  $T$  the temperature (K),  $\eta$  the viscosity (Pa.s), and  $\lambda$  the translation distance of the diffusing ion ( $\text{\AA}$ ). This apparent contradiction can be explained since  $D$  in the Eyring's law refers to the mobility of the  $\text{SiO}_2$  framework and not to the mobility of the alkali.

The positive effect of water on the electrical conductivity was clearly observed in this study. The magnitude of the effect of water is comparable to the one observed by *Gaillard* [2004] on rhyolitic melts. The conductivity enhancement was attributed to the effect of water incorporation in the rhyolitic melt on the mobility of Na. We can therefore anticipate that the increase in conductivity as water is incorporated in our melts reflects an enhancement of Na-mobility as well. Protons are not expected to contribute to the ionic conductivity in natural melts because hydrogen has been shown to move as neutral molecules (either  $\text{H}_2\text{O}$  or  $\text{H}_2$ ) in alumino-silicate melts [*Zhang and Stolper*, 1991; *Gaillard et al.*, 2003; *Behrens et al.*, 2004]. *Behrens et al.* [2002] proposed that for hydrous  $\text{BaSi}_2\text{O}_5$  glass,  $\text{H}^+$  could significantly contribute to the measured conductivity, and attributed this finding to the strongly depolymerised character ( $\text{NBO}/\text{T}=1.5$ ) of the studied glass. However, the effectiveness of proton migration in silicate melts and its possible contribution to electrical charge transfer remain debated.

Because of the presence of iron in our samples, electronic conductivity can also occur, particularly in the glass region [*Cooper et al.*, 1996]. For instance, *Barczynski and Murawski* [2002] demonstrated that iron-rich glasses (from 20 to 32 wt% of FeO) are good electronic conductors at low  $T$ , and that small polaron hopping is a possible charge carrier transport process in such glasses. However, the Fe content of our three studied samples is much lower than in *Barczynski and Murawski* [2002]. In addition, the mean interatomic distance of iron in our studied materials is greater than 1nm (using chemical compositions from Table 1 and measured densities of anhydrous glasses). At such long distances, charge transfer between iron atoms are not anticipated (H. Behrens, personal communication).

## 5.2. Calculation of electrical conductivity of natural melts

Calculation of the electrical conductivity of natural melts requires three parameters to be specified:  $E_a$ ,  $\sigma_0$  and  $\Delta V$  (Eq. 1). Below, we propose a semi-empirical method allowing the determination of these three parameters, both for the Vesuvius and other natural magmatic liquids.

As the activation energy  $E_a$  in our melts decreases with increasing sodium content and is probably function of the ionic characteristics of the charge carrier (ionic radius, valency, jump distance), we have used the Anderson-Stuart model to compute  $E_a$  values for natural melts [Anderson and Stuart, 1954; Nascimento and Watanabe, 2007 and references therein]. This model, initially based on ionic crystal and elasticity theories, predicts the activation energy of ionic conduction in silicate glasses. The activation energy,  $E_a$ , is expressed as the sum of two energies: the electrostatic binding energy,  $E_b$ , and the strain energy,  $E_s$ , which are expressed as:

$$\begin{aligned} E_a &= E_b + E_s, \\ E_b &= \frac{\beta \cdot z_i \cdot z_o \cdot e^2}{\gamma(r_i + r_o)} \\ E_s &= 4\pi G \lambda (r_i - r_D)^2 \end{aligned} \quad (9)$$

where  $\beta$  is the Madelung constant (taken equal to 0.23, Nascimento and Watanabe [2007]),  $z_i$  the valence of the mobile ion, and  $z_o$  that of the fixed counterion ( $O^{2-}$ ),  $e$  the electronic charge (C),  $\gamma$  the covalency parameter (taken equivalent to the permittivity (F/m), Anderson and Stuart [1954]),  $r_i$  the ionic radius of  $i$  (m),  $r_o$  the ionic radius of the oxygen ion (m),  $G$  the shear modulus (Pa),  $\lambda$  the jumping distance (m) and  $r_D$  the effective radius of the “doorway” through which the sodium passes (taken equal to  $9.3 \cdot 10^{-11}$  m, Nascimento and Watanabe [2007]). In our case,  $i$  corresponds to the sodium, the main charge carrier. Nascimento and Watanabe [2007] have proposed an empirical linear relation between  $\gamma$ ,  $G$  and composition for binary  $SiO_2$ - $K_2O$  glasses. We have assumed that, for our three studied compositions,  $\gamma$  and  $G$  vary linearly with the sodium content. Regressions of our data yield the following two empirical equations for  $\gamma$  and  $G$ :

$$\begin{cases} G = -2.107 \cdot 10^{11} \cdot wt\%Na_2O + 1.297 \cdot 10^{12} \\ \gamma = 2.439 \cdot 10^{-11} \cdot wt\%Na_2O + 1.720 \cdot 10^{-10} \end{cases} \quad (10)$$

Since our data clearly show a decrease in  $E_a$  with increasing water content (Table 3), a water term has been added in the expression of  $E_a$ . The effect of the addition of water was considered to be essentially mechanical, inducing a local dilatation effect of the structure, allowing  $Na^+$  ions to move more freely. Consequently, a modification of the  $E_s$  term was introduced, since  $E_s$  describes the mechanical forces applied on the charge carrier [Nascimento and Watanabe, 2007]. The strain energy  $E_s$  of hydrous melts can be written as:

$$E_s = 4\pi G \lambda (r_{Na} - r_D)^2 + 1000 \cdot (wt\%H_2O)^2 \quad (11)$$

where wt%H<sub>2</sub>O is the water content of the melt (wt%). Ea calculated from the Anderson-Stuart model (Eq. 9 to 11) are in good agreement with Ea determined for the three Vesuvius melt compositions (Table 3). Measured activation energies are reproduced with a correlation coefficient of 0.999 and an average error of 3% relative.

The pre-exponential term ( $\sigma_0$ ) was calculated using the compensation law (Eq.7) applied to our compositions, with Ea calculated with Eq.9 to 11.

The Arrhenius laws obtained for the different experiments show grouped  $\Delta V$  values (Table 3). Consequently, we have assumed that the  $\Delta V$  term is independent of composition and water contents.  $\Delta V$  was fitted from our experimental conductivity data with Ea being calculated from Eq. 9 to 11 and  $\sigma_0$  from the compensation law. This yields an activation volume of  $2 \cdot 10^{-5} \text{ m}^3/\text{mol}$  (i.e.  $20 \text{ cm}^3/\text{mol}$ ), in the middle of the range of  $\Delta V$  values of the Arrhenian equations (Table 3). The model (with Ea calculated using the Anderson-Stuart formalism,  $\sigma_0$  from the compensation law and  $\Delta V=20 \text{ cm}^3/\text{mol}$ ) reproduces measured conductivity values with a correlation coefficient of 0.985 and an average error of 11% relative. We have also tested the model against conductivity data from *Presnall* [1972], *Tyburczy and Waff* [1983, 1985], *Satherley and Smedley* [1985, dry lava], *Park and Ducea* [2003], *Gaillard* [2004] and *Gaillard and Iacono Marziano* [2005]. We did not consider data from Na diffusion here. Indeed, the calculation of conductivities from Na diffusion using the Nernst-Einstein equation did not constrain sufficiently the value of  $\sigma$ , because of the lack of data about the value of the Haven ratio. The data of conductivity studies are reproduced with a difference less than 0.5 log-unit (except for the data about the tholeiite from Tyburczy and Waff and for the data of Gaillard and Giacono Marziano, which are reproduced with a difference between 0.5 and 0.7 log-unit). We conclude that the above model is able to calculate the electrical conductivity of common natural melts. Since Eq. 7 and 11 have been established for water contents ranging from 0 to 6 wt%, use of the model above 6 wt% is not recommended, since an increase of the water content of the melt can have a dilution effect on Na which, thus, may influence the conductivity [*Gaillard*, 2004]. In the same way, extrapolation of the model at pressures significantly above 400 MPa is not recommended, since experimental calibrating data are lacking above 400 MPa.

### 5.3. Volcanological implications for Mt. Vesuvius

As demonstrated by *Roberts and Tyburczy* [1999], the Archie's law conduction model may be used to estimate the electrical conductivity of magmatic suspensions. *Glover et al.*

[2000] proposed the following equation to calculate the conductivity of a magma over the whole melt fraction range, knowing the individual conductivities of the crystals and the liquid:

$$\sigma_{magma} = \sigma_{cr} \cdot (x_{cr})^{\left(\frac{\log(1-(x_{liq})^m)}{\log(1-x_{liq})}\right)} + \sigma_{liq} \cdot (x_{liq})^m \quad (11),$$

where  $\sigma_{liq}$  is the conductivity of the liquid,  $\sigma_{cr}$  is the conductivity of crystals,  $\sigma_{magma}$  is the conductivity of the corresponding magma,  $x_{liq}$  and  $x_{cr}$  are the proportions (volume fraction) of the liquid and the crystals, respectively ( $x_{liq} = 1 - x_{cr}$ ) and  $m$  the Archie cementation exponent. We used  $m=1.05$  [Gaillard and Iacono Marziano, 2005]. For the case of Mt. Vesuvius magmas, crystals considered are mixtures of leucite and clinopyroxenes. Tyburczy and Fisler [1995] provide data on the electrical conductivity of these two mineral phases as a function of temperature. The electrical conductivity of the pure liquid phase is calculated by using an Arrhenian formalism, with  $E_a$  from Eq. 9-11 and  $\sigma_0$  from the compensation law applied to our melts.

Using the modified Archie's law, the electrical conductivity of tephritic to phonolitic magmas can be estimated during crystallization. Typical phenocryst contents of Vesuvius eruptions ranges between 10 and 20% [Rosi and Santacroce, 1983; Cioni et al., 1995]. Phenocryst modes of 50%Cpx and 50%Lc are assumed. For the phonolitic magma erupted during the Pompei eruption, the electrical conductivity calculations were carried out for a temperature of 815°C and a melt water concentration of 6 wt%H<sub>2</sub>O [Cioni et al., 1995; Scaillet et al., 2007]. At a pressure of 200 MPa, conductivities calculated with the modified Archie's law range between 0.60 to 0.80 (Ohm.m)<sup>-1</sup>. For the tephriphonolitic magma erupted during the Pollena eruption, a calculated conductivity range of 0.95-1.10 (Ohm.m)<sup>-1</sup> was obtained for a temperature of 1050°C, a pressure of 200 MPa and a melt water content of 3.5 wt% [Scaillet et al., 2007]. For the tephritic magma, the calculated conductivity ranges between 0.40 and 0.60 (Ohm.m)<sup>-1</sup>, for a temperature of 1100°C, a pressure of 200 MPa and a melt water content of 3 wt%. For comparison, the present models of electrical conductivity below Mt. Vesuvius yield a maximal value of ~1.30 (Ohm.m)<sup>-1</sup> [Di Maio, 1998; Petrillo, unpublished data]. Therefore, there is no strict overlap between electrical conductivities measured below Mt. Vesuvius and values typical of magmas involved in the past activity of the volcano. However, this should not be taken to indicate the present-day absence of magma beneath Mt. Vesuvius. The typical spatial resolution of MT measurements does not rule out the possibility of the presence of a small magma reservoir. In addition, the magma-wall rock interface may be complex, with the presence of hydrothermal circulations and of a

metasomatised thermal aureole [e.g. *Fulignati et al., 2004; 2005*], which would hamper the identification of magma from the inversion of the MT data. Yet, we note that the magmatic conductivity value the closest to the maximum measured from MT studies concerns the tephriphonolitic magma. Current models for Mt. Vesuvius favour a future eruption of tephriphonolite magma similar to the Pollena event [*Santacroce et al., 1987; 2005*]. Increasing the crystal content of the magma above 20% or increasing the Lc/Cpx proportion above 1 would partially bridge the gap between magma and electrical conductivities measured by MT studies. The MT results could thus be compatible with a low-temperature crystal-rich magmatic system, consistent with the interpretations of seismic tomography data [*Zollo et al., 1998; Auger et al., 2001*].

## 6. Conclusions

Electrical impedance measurements have been used to discriminate the effects of temperature, pressure, and chemical composition, including water content, on the electrical response of three magmas from Mt. Vesuvius. Data were obtained in both the glass and melt regions. The conductivity increases with increasing temperature, melt water content and degree of polymerisation of the melt and decreases with pressure.

Electrical conductivity was identified to be essentially controlled by sodium migration in both the glass and melt regions. Data were fitted by Arrhenius laws, yielding activation energies ( $E_a$ ) and activation volumes ( $\Delta V$ ) ranging from 61 to 142 kJ/mol and 16 to 24 cm<sup>3</sup>/mol, respectively. Data from this and other studies were used to formulate a general compensation law, relating  $E_a$  and  $\sigma_0$ , valid over a wide compositional range.

A semi-empirical method allowing the determination of  $E_a$ ,  $\sigma_0$  and  $\Delta V$  for natural magmatic liquids was constructed on the basis of our experimental data. The activation energy is modelled successfully on the basis of the Anderson-Stuart model,  $\sigma_0$  is obtained from the compensation law and  $\Delta V$  is fitted from our experimental conductivity data. The model enables the electrical conductivity to be calculated for the entire range of melt compositions at Mt. Vesuvius. It also predicts satisfactorily the electrical response of other melt compositions.

The laboratory-based electrical conductivity data for Mt. Vesuvius melts and magmas yield values slightly lower than the electrical anomaly revealed by MT studies performed at Mt. Vesuvius. Future modelling of the deep structure of Mt. Vesuvius on the basis of

electrical measurements will have to integrate results from this study for the Vesuvius magmas.

## Acknowledgments

This paper is part of the PhD of A. Pommier. The authors are grateful to P. Marianelli for providing the sample VS88-65B and R. Cioni for the sample VES9. We also thank J-M Bény for his help in FTIR analyses. This study has been supported by the French national agency for research, ANR JC05-42707 (Electrovolc) attributed to F. Gaillard.

## References

- Alibert, C., and J. P. Carron (1980), Données expérimentales sur la diffusion des éléments majeurs entre verres ou liquides de compositions basaltique, rhyolitique et phonolitique, entre 900°C et 1300°C, à pression ordinaire, *Earth and Planetary Science Letters*, 47(2), 294-306.
- Anderson O.L., and D.A. Stuart (1954), Calculation of activation energy of ionic conductivity in silica glasses by classical methods, *Journal of American Society*, 37 (12), 573-580.
- Angell, C. A. (2001), Glass transition, in *Encyclopaedia of materials : science and technology*, eds. Buschow et al., Vol.4, pp. 3565-3575, Elsevier, Amsterdam.
- Auger, E., P. Gasparini, J. Virieux, and A. Zollo (2001), Seismic evidence of an extended magmatic sill under Mt. Vesuvius, *Science*, 294(5546), 1510-1512.
- Ayuso, R. A., B. De Vivo, G. Rolandi, R.R. Seal, and A. Paone (1998), Geochemical and isotopic (Nd-Pb-Sr-O) variations bearing on the genesis of volcanic rocks from Vesuvius, Italy, *Journal of Volcanology and Geothermal Research*, 82(1-4), 53-78.
- Bagdassarov, N., H. C. Freiheit, and A. Putnis (2001), Ionic conductivity and pressure dependence of trigonal-to-cubic phase transition in lithium sodium sulphate, *Solid State Ionics*, 143(3-4), 285-296.
- Bagdassarov, N. S., J. Maumus, B. Poe, A. B. Slutskiy, and V. K. Bulatov (2004), Pressure dependence of Tg in silicate glasses from electrical impedance measurements, *Physics and Chemistry of Glasses*, 45(3), 197-214.
- Barczynski, R. J., and L. Murawski (2002), Mixed electronic-ionic conductivity in transition metal oxide glasses containing alkaline ions, *Journal of Non-Crystalline Solids*, 307, 1055-1059.

Behrens, H., C. Romano, M. Nowak, F. Holtz, and D. B. Dingwell (1996), Near-infrared spectroscopic determination of water species in glasses of system  $\text{MAlSi}_3\text{O}_8$  (M=Li, Na, K): An interlaboratory study, *Chemical Geology*, 128(1-4), 41-63.

Behrens, H., R. Kappes, and P. Heitjans (2002), Proton conduction in glass - an impedance and infrared spectroscopic study on hydrous  $\text{BaSi}_2\text{O}_5$  glass, *Journal of Non-Crystalline Solids*, 306(3), 271-281.

Behrens, H., Y. Zhang, and Z. Xu (2004),  $\text{H}_2\text{O}$  diffusion in dacitic and andesitic melts, *Geochimica et Cosmochimica Acta*, 68(24), 5139-5150.

Brasse, H., P. Lezaeta, V. Rath, K. Schwalenberg, W. Soyer, and V. Haak (2002), The Bolivian Altiplano conductivity anomaly, *Journal of Geophysical Research-Solid Earth*, 107(B5), 17.

Caillot, E., M. J. Duclot, J. L. Souquet, M. Levy, F. G. K. Baucke, and R. D. Werner (1994), A unified model for ionic transport in alkali disilicates below and above the glass transition, *Physics and Chemistry of Glasses*, 35(1), 22-27.

Cioni, R., L. Civetta, P. Marianelli, N. Metrich, R. Santacroce, and A. Sbrana (1995), Compositional layering and syn-eruptive mixing of a periodically refilled shallow magma chamber : the AD 79 Plinian eruption of Vesuvius, *Journal of Petrology*, 36(3), 739-776.

Cooper, R. F., J. B. Faselow, and D. B. Paker (1996), The mechanism of oxidation of a basaltic glass : chemical diffusion of network-modifying cations, *Geochimica et Cosmochimica Acta*, 60(17), 3253-3265.

Crank, J. (1975), The mathematics of diffusion, Second Ed., *Oxford Scientific Publications*, ISBN 2-86883-447-7, 440p.

Déportes, C., M. Duclot, P. Fabry, J. Fouletier, A. Hammou, M. Kleitz, E. Siebert, and J.L. Souquet (1994), *Electrochimie des solides*, Collection Grenoble Sciences, Pug, Grenoble, 437p.

Di Carlo, I., M. Pichavant, S. G. Rotolo, and B. Scaillet (2006), Experimental crystallization of a high-K arc basalt: The golden pumice, Stromboli volcano (Italy), *Journal of Petrology*, 47(7), 1317-1343.

Di Maio, R., P. Mauriello, D. Patella, Z. Petrillo, S. Piscitelli, and A. Siniscalchi (1998), Electric and electromagnetic outline of the Mount Somma-Vesuvius structural setting, *Journal of Volcanology and Geothermal Research*, 82(1-4), 219-238.

Dingwell, D. B. (1995), Relaxation in silicate melts: Some applications, in *Structure, Dynamics and Properties of Silicate Melts*, pp. 21-66, Mineralogical Soc America, Washington.

Fulignati, P., P. Marianelli, R. Santacroce, and A. Sbrana (2004), Probing the Vesuvius magma chamber – host rock interface through xenoliths, *Geology Magazine*, 141 (4), 417-428.

Fulignati, P., C. Panichi, A. Sbrana, S. Caliro, A. Gioncada, and A. Del Moro (2005), Skarn formation at the walls of the 79AD magma chamber of Vesuvius (Italy): Mineralogical and isotopic constraints, *Neues Jahrbuch fur Mineralogie, Abhandlungen*, 181 (1), 1-10.

Gaillard, F., B. Scaillet, M. Pichavant, and J. M. Beny (2001), The effect of water and  $\text{fO}_2$  on the ferric-ferrous ratio of silicic melts, *Chemical Geology*, 174(1-3), 255-273.

Gaillard, F., B. Schmidt, S. Mackwell, and C. McCammon (2003), Rate of hydrogen-iron redox exchange in silicate melts and glasses, *Geochimica et Cosmochimica Acta*, 67 (13), 2427-2441.

Gaillard, F. (2004b), Laboratory measurements of electrical conductivity of hydrous and dry silicic melts under pressure, *Earth and Planetary Science Letters*, 218(1-2), 215-228.

Gaillard, F., and G. I. Marziano (2005), Electrical conductivity of magma in the course of crystallization controlled by their residual liquid composition, *Journal of Geophysical Research-Solid Earth*, 110(B6), 12.

Glover, P. W. J., M. J. Hole, and J. Pous (2000), A modified Archie's law for two conducting phases, *Earth and Planetary Science Letters*, 180(3-4), 369-383.

Heinemann, I., and G. H. Frischat (1993), The sodium transport mechanism in  $\text{Na}_2\text{O}\cdot 2\text{SiO}_2$  glass determined by the Chemla experiment, *Physics and Chemistry of Glasses*, 34 (6), 255-260.

Henderson, P., J. Nolan, G. C. Cunningham, and R. K. Lowry (1985), Structural control and mechanisms of diffusion in natural silicate melts, *Contributions to Mineralogy and Petrology*, 89(2-3), 263-272.

Hess, K. U., and D. B. Dingwell (1996), Viscosities of hydrous leucogranitic melts: A non-Arrhenian model, *American Mineralogist*, 81(9-10), 1297-1300.

Hoffmann-Rothe, A., O. Ritter, V. Haak (2001), Magnetotelluric and geomagnetic modelling reveals zones of very high electrical conductivity in the upper crust of Central Java, *Physics of the Earth and Planetary Interiors*, 124(3-4), 131-151.

Huebner, J. S., and R. G. Dillenburg (1995), Impedance spectra of hot, dry silicate minerals and rock: qualitative interpretation of spectra, *American Mineralogist*, 80(1-2), 46-64.

Jambon, A. (1982), Tracer diffusion in granitic melts: experimental results for Na, K, Rb, Cs, Ca, Sr, Ba, Ce, Eu, to 1300°C and a model of calculation, *Journal of Geophysical Research-Solid Earth*, 87(B13), 10797-10810.

Jones, A. G. (1999), Imaging the continental upper mantle using electromagnetic methods, *Lithos*, 48(1-4), 57-80.

Kress, V. C., and M. S. Ghiorso (1993), Multicomponent diffusion in basaltic melts, *Geochimica et Cosmochimica Acta*, 57(18), 4453-4466.

Malki, M., and P. Echegut (2003), Electrical conductivity of the CaO-SiO<sub>2</sub> system in the solid and the molten states, *Journal of Non-Crystalline Solids*, 323, 131-136.

Manzella, A., G. Volpi, A. Zaja, and M. Meju (2004), Combined TEM-MT investigation of shallow-depth resistivity structure of Mt Somma-Vesuvius, *Journal of Volcanology and Geothermal Research*, 131(1-2), 19-32.

Maumus, J., N. Bagdassarov, and H. Schmeling (2005), Electrical conductivity and partial melting of mafic rocks under pressure, *Geochimica et Cosmochimica Acta*, 69(19), 4703-4718.

Mungall, J. E. (2002), Empirical models relating viscosity and tracer diffusion in magmatic silicate melts, *Geochimica et Cosmochimica Acta*, 66 (1), 125-143.

Mysen, M. O., and P. Richet (2005), *Silicate glasses and melts, Properties and structure*, Elsevier, Amsterdam, 544p.

Nascimento M.L.F., and S. Watanabe (2007), Test of the Anderson-Stuart model and correlation between free volume and the 'universal' conductivity in potassium glasses, *Materials Chemistry and Physics*, 105, 308-314.

Nell, J., B. J. Wood, and T. O. Mason (1989), High-temperature cation distributions in  $\text{Fe}_3\text{O}_4\text{-MgAl}_2\text{O}_4\text{-MgFe}_2\text{O}_4\text{-FeAl}_2\text{O}_4$  spinels from thermopower and conductivity measurements, *American Mineralogist*, 74(3-4), 339-351.

Nunziata, C., M. Natale, G. Luongo, and G.F. Panza (2006), Magma reservoir at Mt. Vesuvius: Size of the hot, partially molten, crust material detected deeper than 8 km, *Earth and Planetary Science Letters*, 242(1-2), 51-57.

Park, S. K., and M. N. Ducea (2003), Can in situ measurements of mantle electrical conductivity be used to infer properties of partial melts?, *Journal of Geophysical Research-Solid Earth*, 108(B5), 2270.

Partzsch, G. M., F. R. Schilling, and J. Arndt (2000), The influence of partial melting on the electrical behavior of crustal rocks: laboratory examinations, model calculations and geological interpretations, *Tectonophysics*, 317(3-4), 189-203.

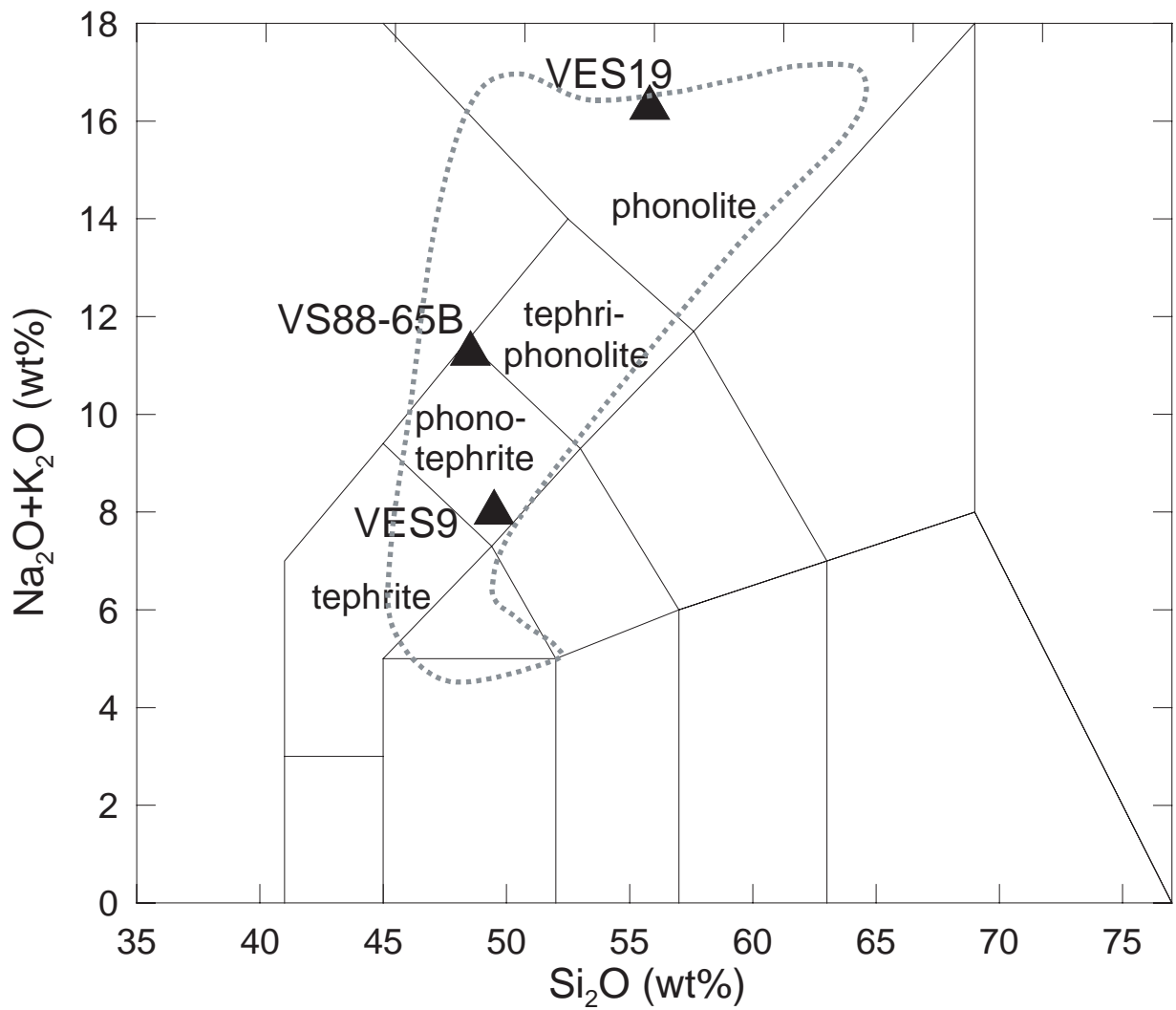
- Pfeiffer, T. (1998), Viscosities and electrical conductivities of oxidic glass-forming melts, *Solid State Ionics*, 105, 277-287.
- Presnall, D. C., C. L. Simmons, and H. Porath (1972), Change in electrical conductivity of a synthetic basalt during melting, *Journal of Geophysical Research-Solid Earth*, 77(29), 5665-5672.
- Reid, J. E., B. T. Poe, D. C. Rubie, N. Zotov, and M. Wiedenbeck (2001), The self-diffusion of silicon and oxygen in diopside (CaMgSi<sub>2</sub>O<sub>6</sub>) liquid up to 15GPa, *Chemical Geology*, 174, 77-86.
- Roberts, J. J., and J. A. Tyburczy (1994), Frequency dependent electrical properties of minerals and partial-melts, *Surveys in Geophysics*, 15(2), 239-262.
- Roberts, J. J., and J. A. Tyburczy (1999), Partial-melt electrical conductivity: Influence of melt composition, *Journal of Geophysical Research-Solid Earth*, 104(B4), 7055-7065.
- Roling, B. (1999), What do electrical conductivity and electrical modulus spectra tell us about the mechanisms of ion transport processes in melts, glasses, and crystals?, *Journal of Non-Crystalline Solids*, 244(1), 34-43.
- Rosi, M., and R. Santacroce (1983), The AD 472 "Pollena" eruption: volcanological and petrological data for this poorly-known, Plinian-type event at Vesuvius, *Journal of Volcanology and Geothermal Research*, 17(1-4), 249-271.
- Rosi, M., C. Principe, and R. Vecci (1993), The 1631 Vesuvius eruption. A reconstruction based on historical and stratigraphical data, *Journal of Volcanology and Geothermal Research*, 58, 151-182.
- Santacroce, R. (Ed) (1987), Somma-Vesuvius, *CNR Quaderni della Ricerca Scientifica*, 114 (8), 230p.
- Santacroce, R., R. Cioni, P. Marianelli, and A. Sbrana (2005), Understanding Vesuvius and preparing for its next eruption, in *Cultural responses to the volcanic landscape, The Mediterranean and Beyond*, eds Balmuth et al., pp 27-55, Archeological Institute of America.
- Satherley, J., and S. I. Smedley (1985), The electrical conductivity of some hydrous and anhydrous molten silicates as a function of temperature and pressure, *Geochimica et Cosmochimica Acta*, 49, 769-777.
- Scaillet, B., M. Pichavant, and R. Cioni, *Evidence for the shallowing of the Vesuvius reservoir in the upper crust over the last 20 kyr*, submitted to Nature.
- Scarlato, P., B. T. Poe, C. Freda, and M. Gaeta (2004), High-pressure/high-temperature measurements of electrical conductivity in basaltic rocks from Mount Etna, Sicily, Italy (vol 109, art no B02210, 2004), *Journal of Geophysical Research-Solid Earth*, 109(B4), 1.
- Tyburczy, J. A., and D. K. Fisler (1995), Electrical properties of minerals and melts, *Mineral Physics and Crystallography, A Handbook of Physical Constants*, pp.185-208, AGU, Whashington, D.C.
- Tyburczy, J. A., and H. S. Waff (1983), Electrical conductivity of molten basalt and andesite to 25kilobars pressure: geophysical significance and implications for charge transport and melt structure, *Journal of Geophysical Research*, 88(NB3), 2413-2430.
- Tyburczy, J. A., and H. S. Waff (1985), High pressure electrical conductivity in naturally occurring silicate liquids, in *Point Defects in Minerals, Geophysical Monogr. Ser.*, vol.31, edited by R.N.Shock, pp.78-87, AGU, Whashington, D.C.
- Watson, E. B. (1994), Diffusion in volatile-bearing magmas, in *Volatiles in Magmas*, edited, pp. 371-411, Mineralogical Soc America, Washington.
- Wendlandt, R. F. (1991), Oxygen diffusion in basalt and andesite melts – experimental results and discussion of chemical versus tracer diffusion, *Contributions to Mineralogy and Petrology*, 108(4), 463-471.
- Westrich, H. R. (1987), Determination of water in volcanic glasses by Karl-Fischer titration, *Chemical Geology*, 63(3-4), 335-340.

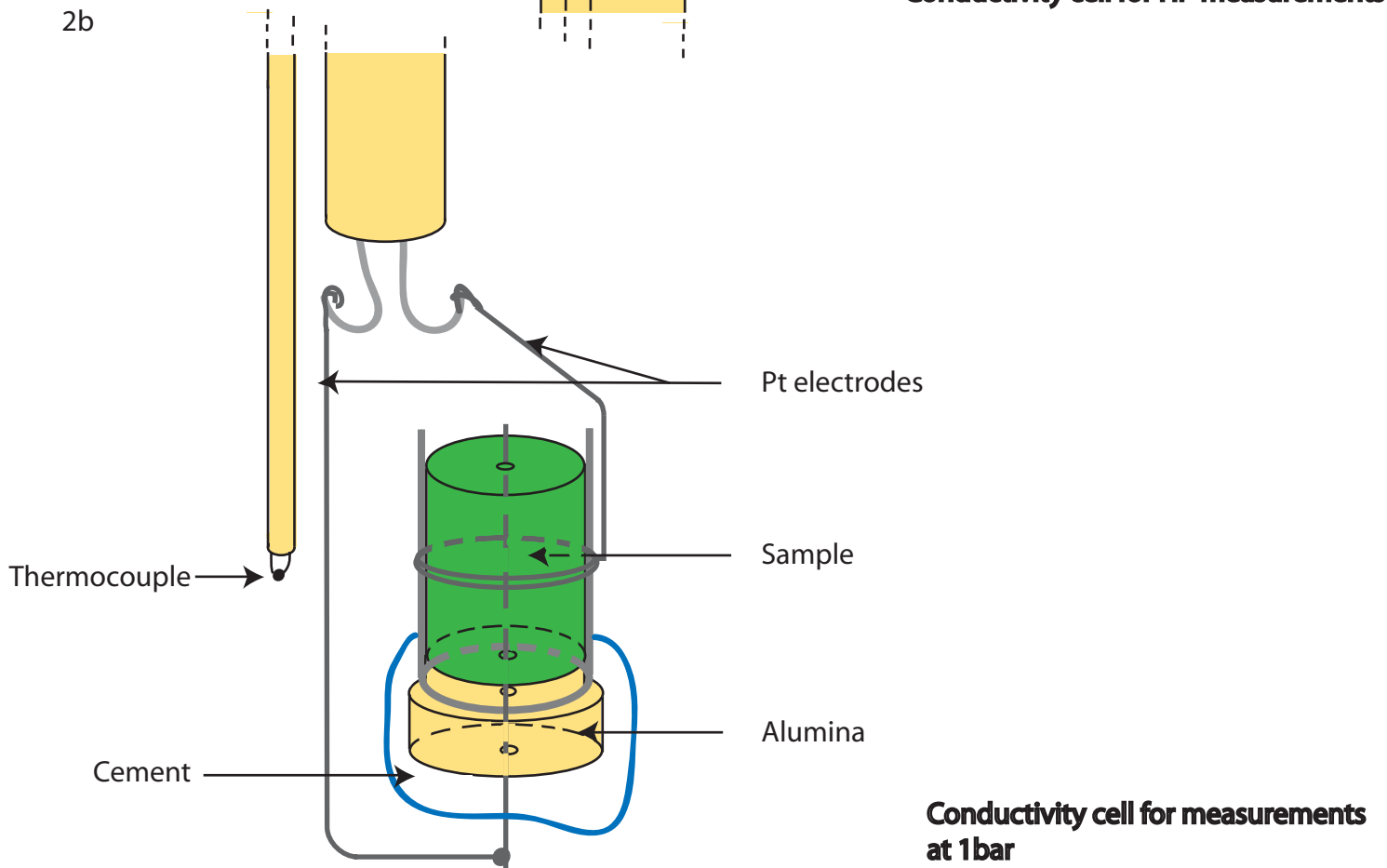
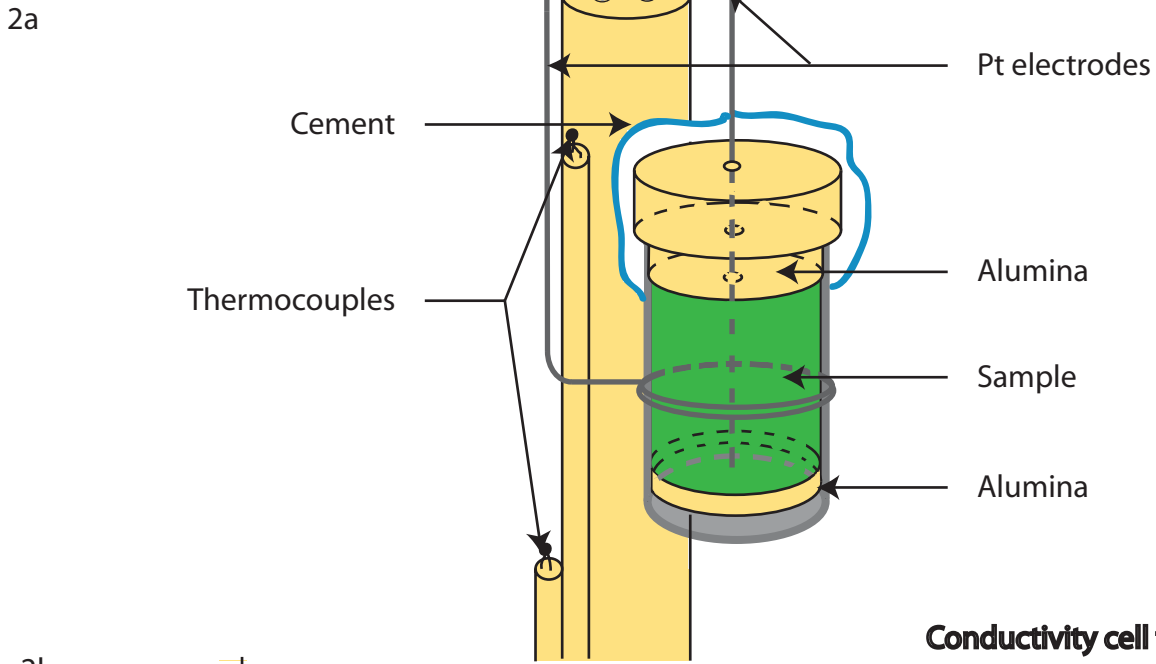
Wu, X., and Y.-F. Zheng (2003), Compensation effect for electrical conductivity and its applications to estimate oxygen diffusivity in minerals, *Journal of Geophysical Research-Solid Earth*, 108(B3), 2139.

Zhang, Y., and E. M. Stolper (1991), Water diffusion in a basaltic melt, *Nature*, 351, 306-309.

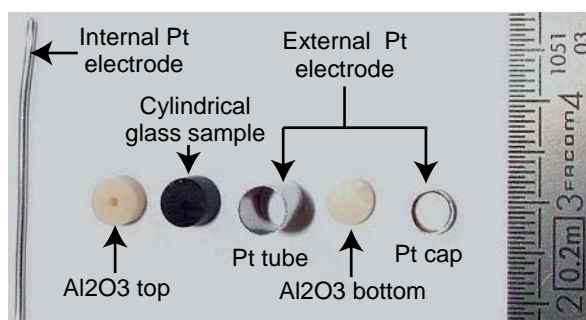
Zollo, A., P. Gasparini, J. Virieux, H. Le Meur, G. deNatale, G. Biella, E. Boschi, P. Capuano, R. De Franco, P. dell'Aversana, R. de Matteis, I. Guerra, G. Iannaccone, L. Mirabile, and G. Vilaro (1996), Seismic evidence for a low-velocity zone in the upper crust beneath Mount Vesuvius, *Science*, 274(5287), 592-594.

Zollo, A., P. Gasparini, J. Virieux, G. Biella, E. Boschi, P. Capuano, R. de Franco, R., P. Dell'Aversana, R. de Matteis, G. De Natale, G. Iannaccone, I. Guerra, H. Le Meur, and L. Mirabile (1998), An image of Mt. Vesuvius obtained by 2D seismic tomography, *Journal of Volcanology and Geothermal Research*, 82(1-4), 161-173.

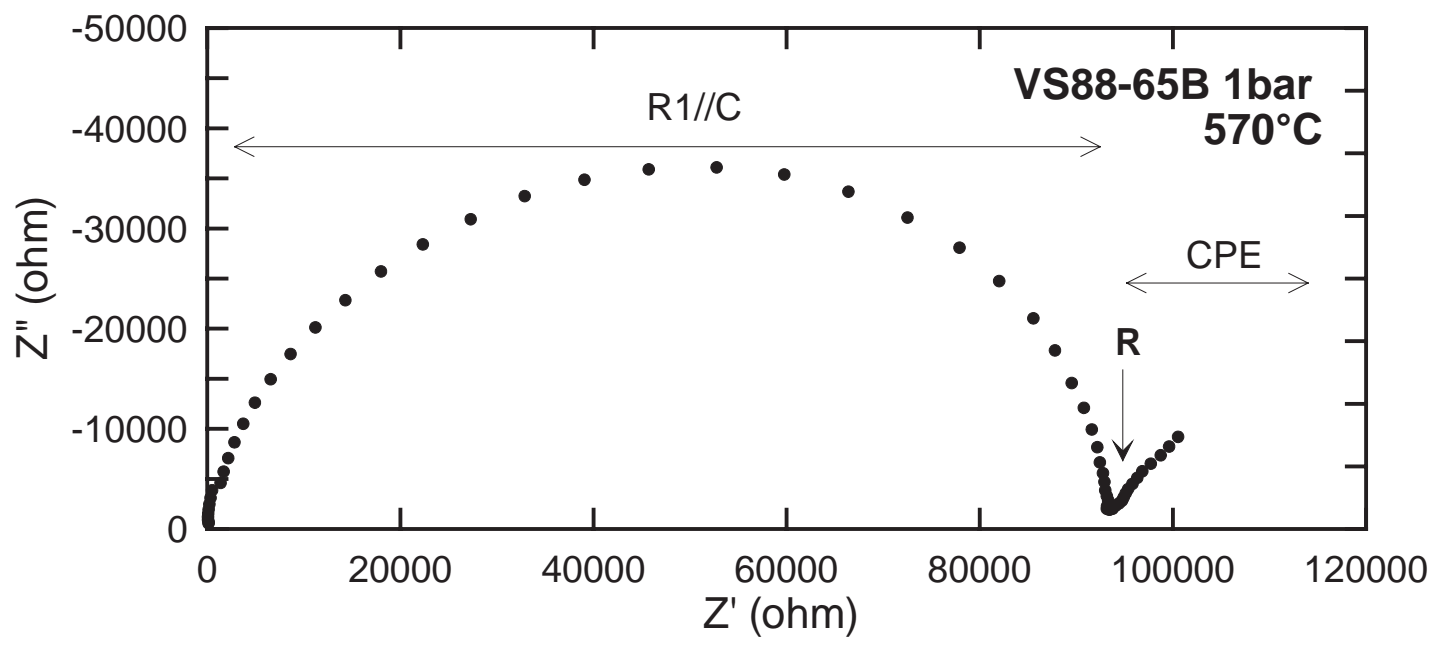




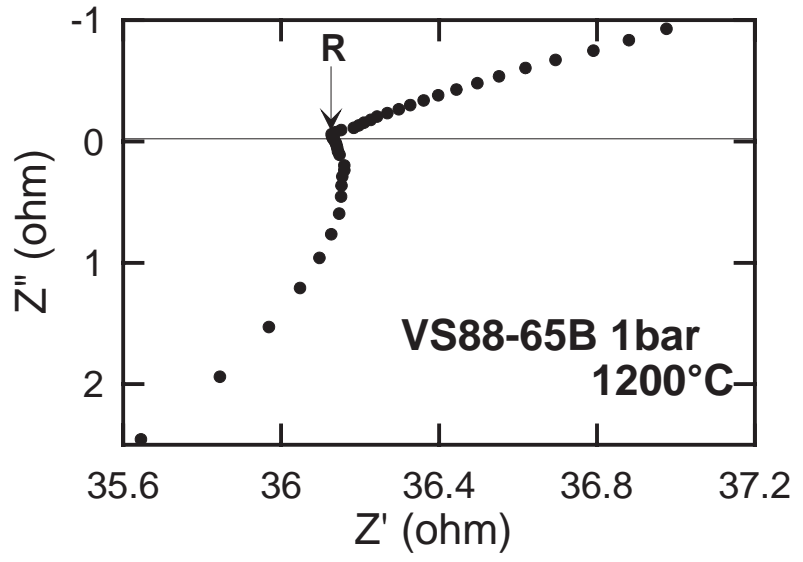
2c



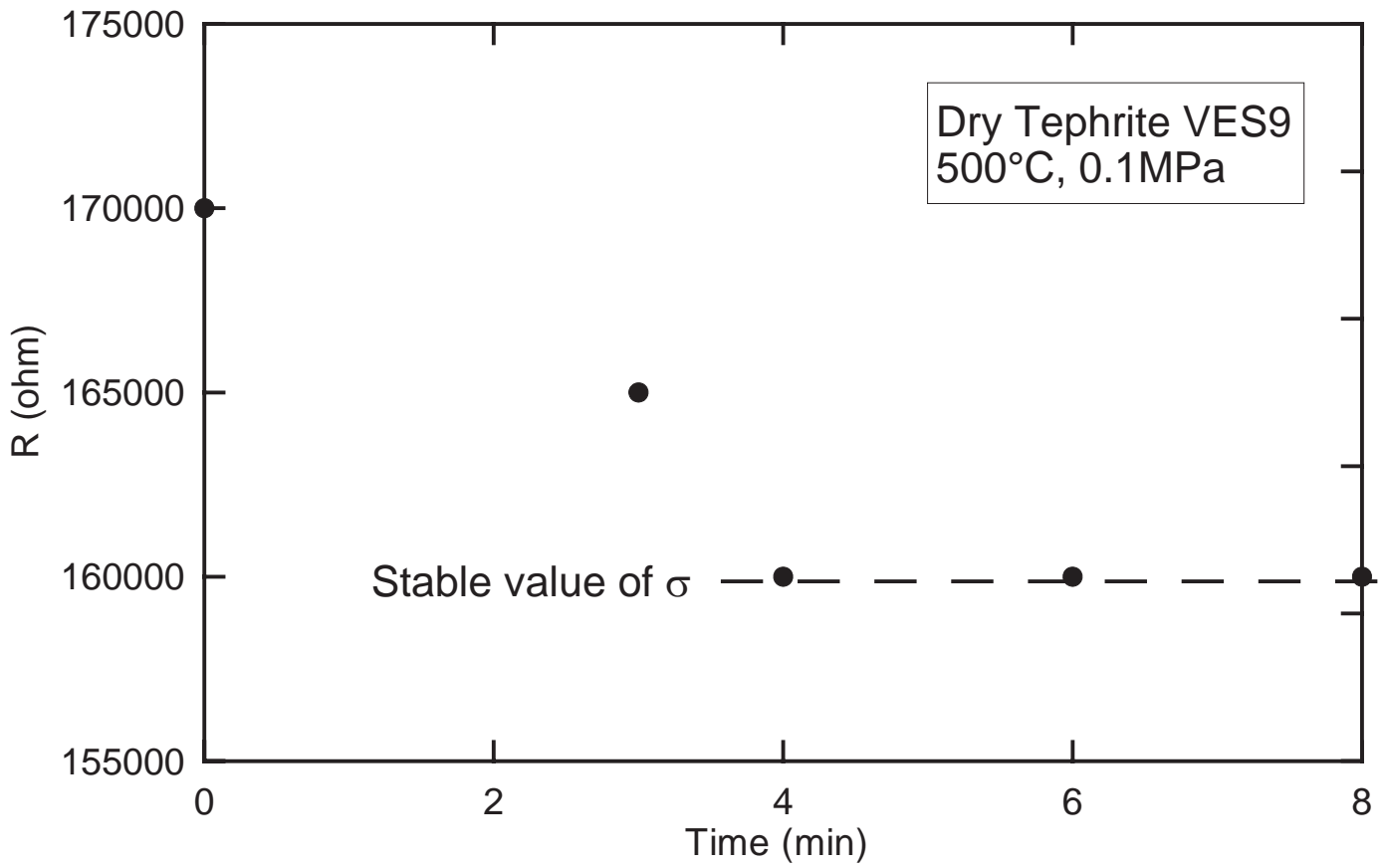
3a



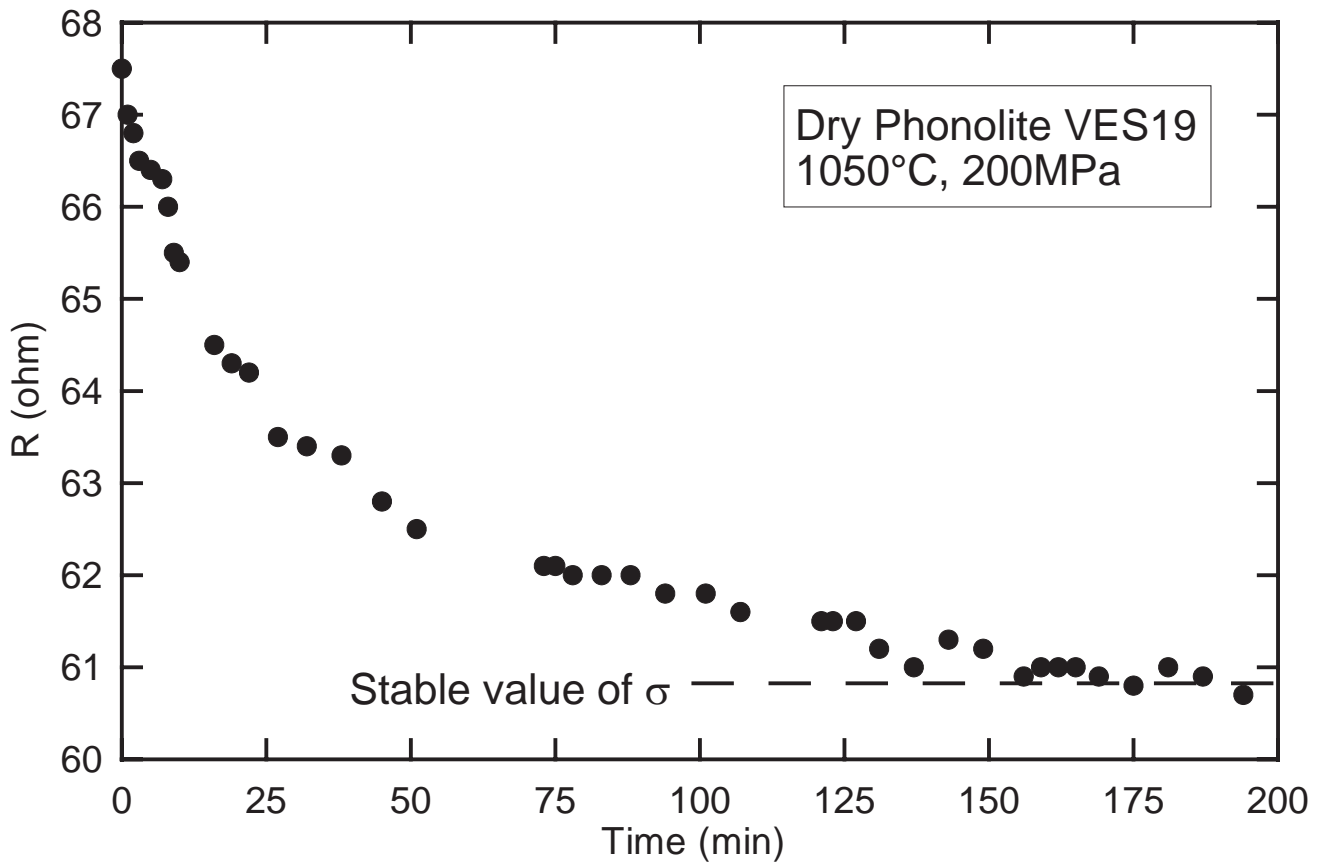
3b

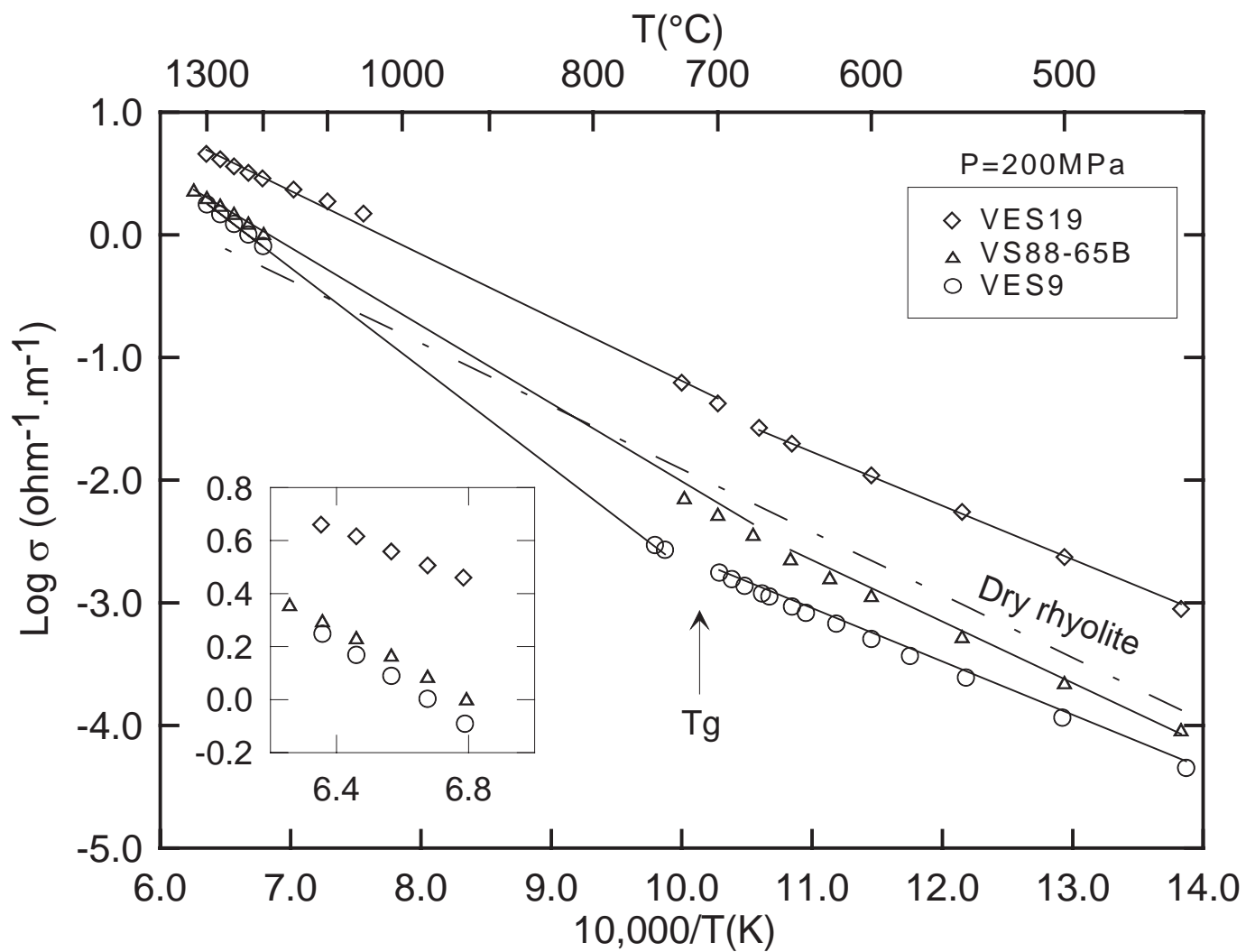


4a

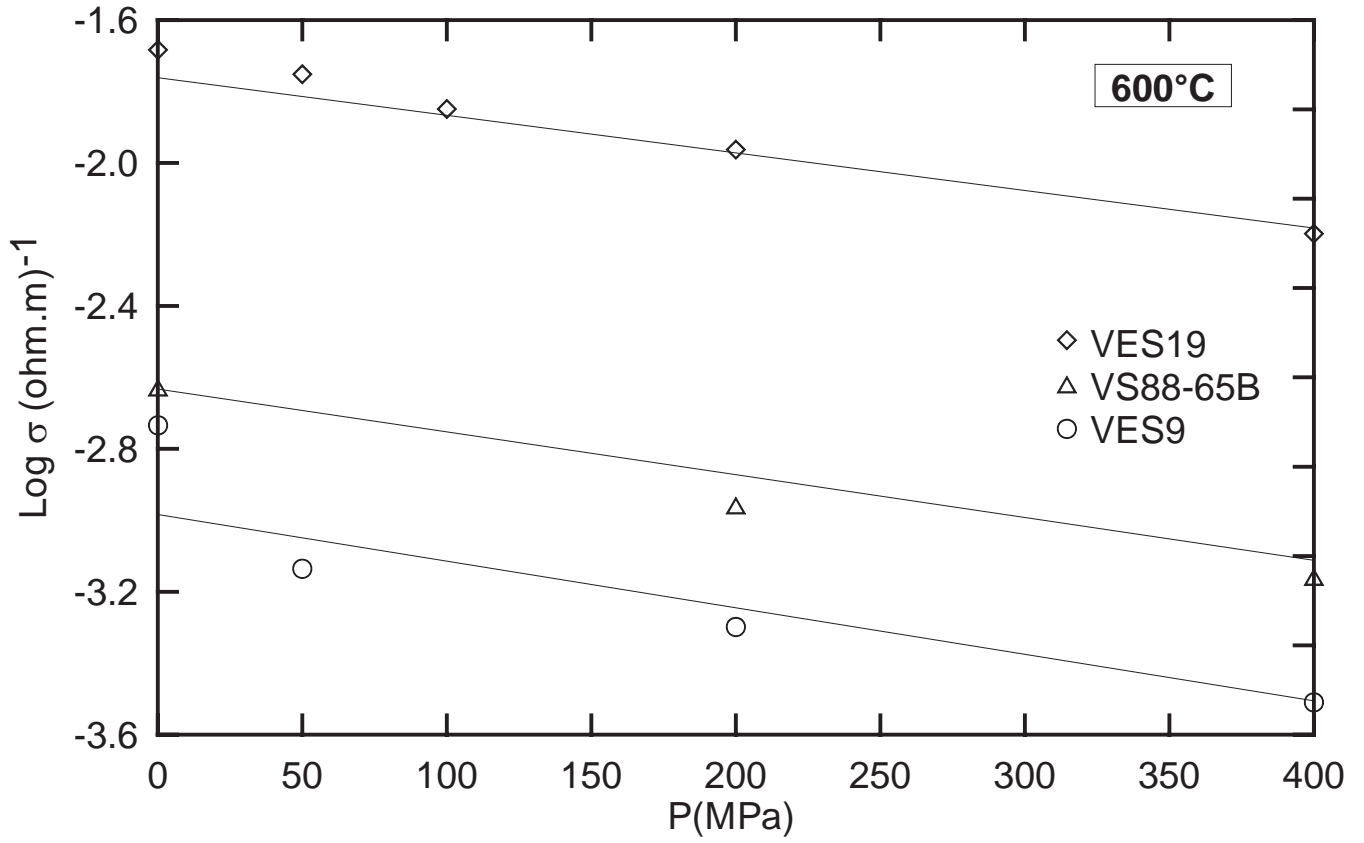


4b

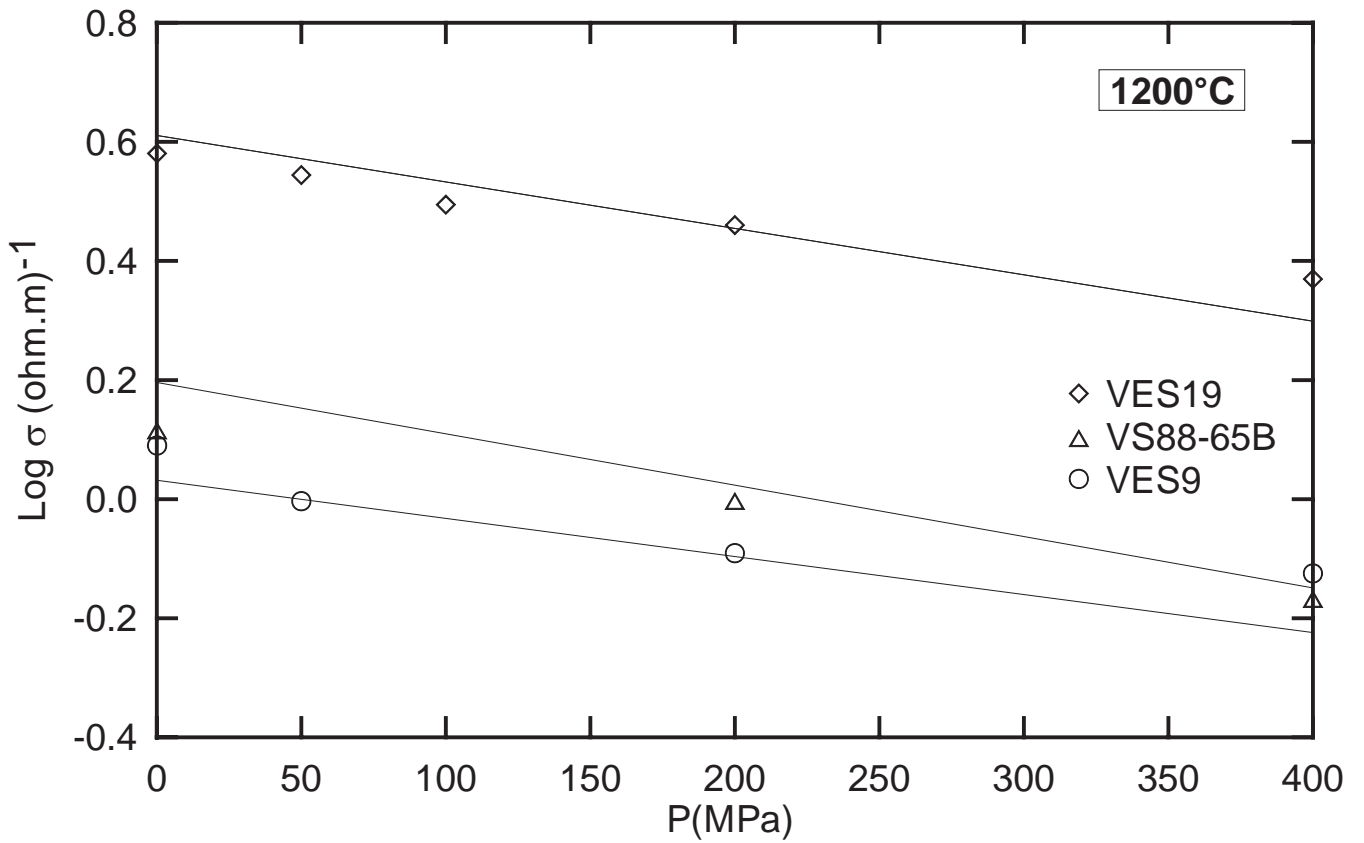




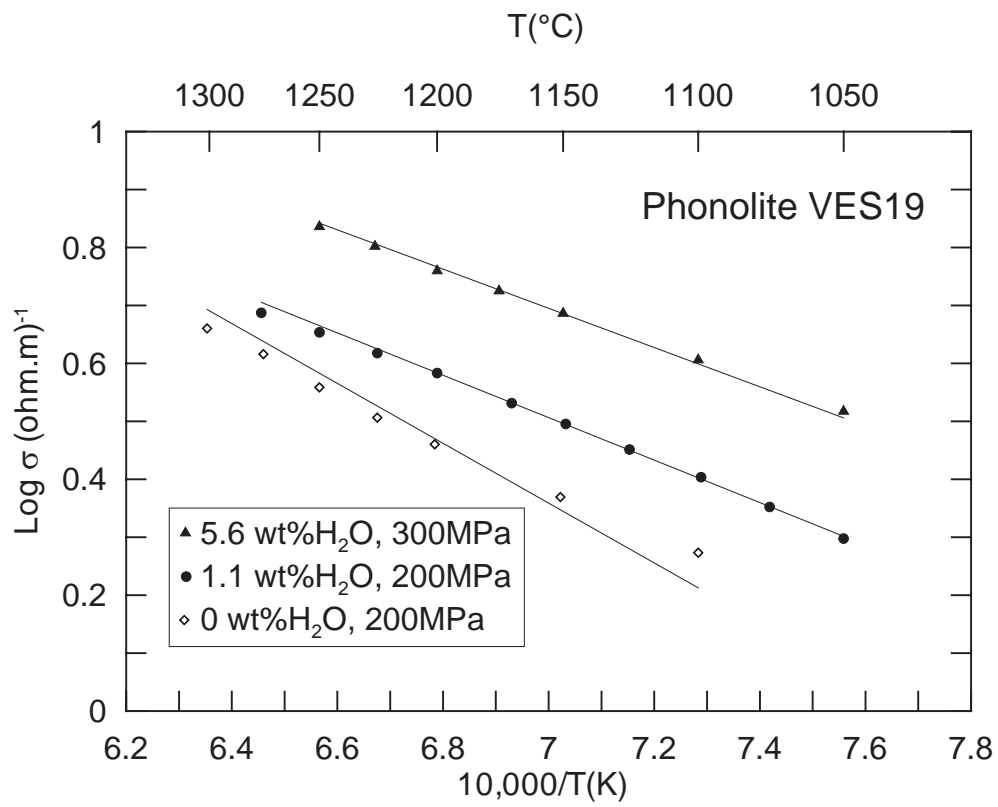
6a



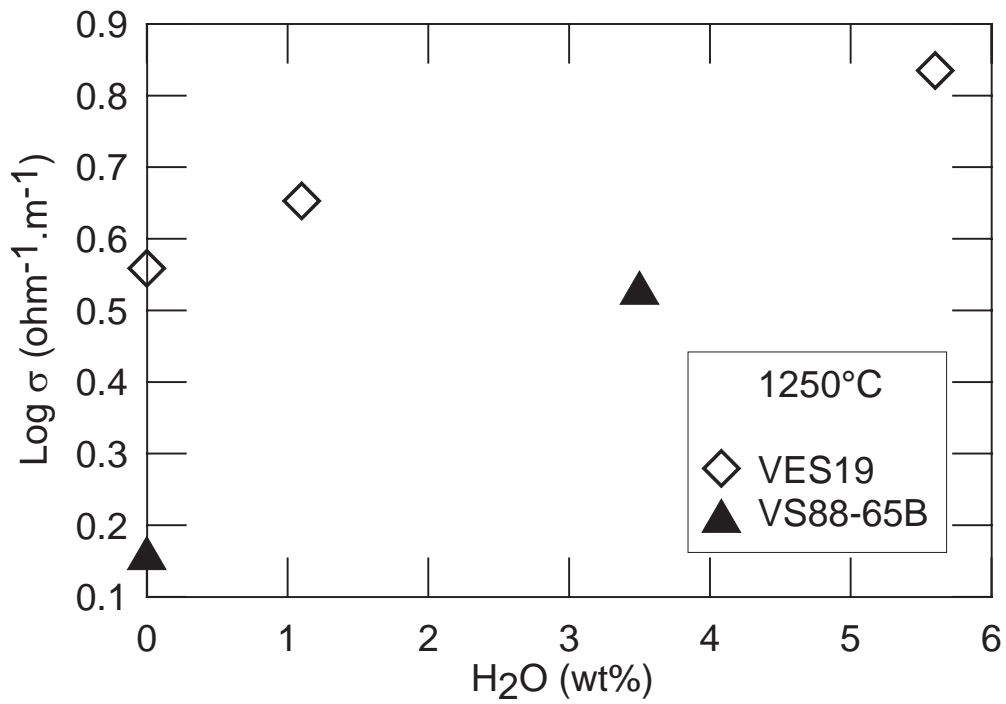
6b



7a



7b



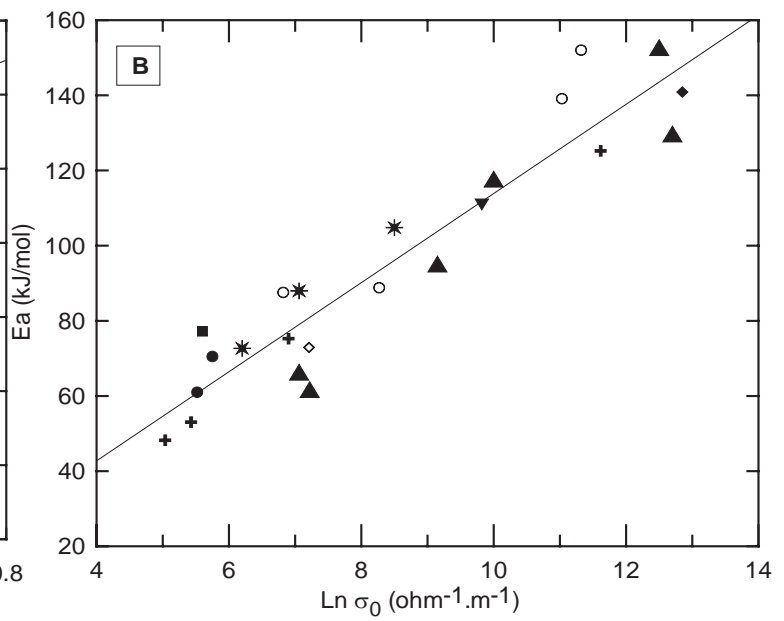
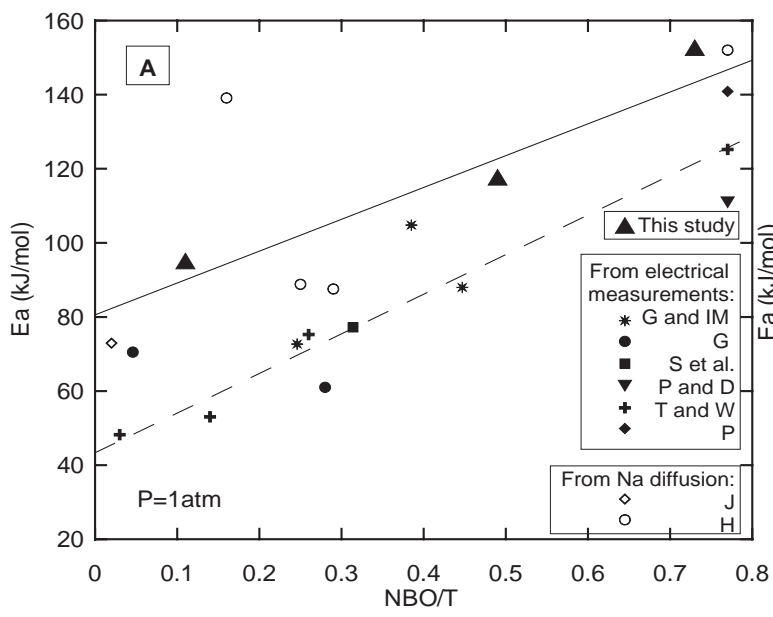


## Figure captions

Figure 1 : Total alkali vs silica (TAS plot) showing the composition of the starting rock samples : tephrite (VES9), phonotephrite (VS88-65B) and phonolite (VES19). See text for provenance of the samples and eruptions. The area delimited by the dashed line is the range of products erupted by Mt. Vesuvius since 10 kyrs [Ayuso et al., 1998].

Figure 2 : Description of the conductivity cells : a) 1 atm cell ; b) high pressure cell ; c) Exploded view of the high pressure conductivity cell showing the glass sample, the Pt tube and cap serving as external electrode, the Pt wire serving as internal electrode and the alumina parts. See text for explanations.

Figure 3 : Electrical responses observed in the Nyquist plan ( $Z'$ ,  $Z''$ ) for the dry phonotephrite sample (VS88-65B) at 1 atm, 570°C (a) and 1 atm, 1200°C (b). The first part of the response (semi-circle, for  $Z' < R$ ) represents the electrical response of the sample while the second part, (mostly linear, for  $Z' > R$ ), represents the effect of the interface between the sample and the electrode. Impedance arcs were observed only at low temperatures (below ~750°C, a). At higher temperatures, no impedance arcs were observed (b).  $R$  (resistance of the sample (ohm)) is obtained for  $Z''=0$  and represents the real part of the complex impedance ( $Z'$ , see text). The electrical response of the sample corresponds to the association of a resistor connected in parallel to a capacitor ( $R1//C$ ) and a Constant Phase Element with another resistor ( $R2+CPE$ ) [Huebner and Dillenburg, 1995].

Figure 4 : Types of evolution of the electrical resistance with time illustrated by the tephrite sample VES9 and the phonolite sample VES19. (a) corresponds to the normal case where a stable value of electrical conductivity is reached in a few minutes. In contrast, in (b), the attainment of a stable conductivity value requires several hours. This behavior is interpreted as reflecting the slow dissolution of pre-existing crystals (in that particular case, most probably leucite) formed during heating up.

Figure 5 : Dependence of the electrical conductivity with temperature for the three samples studied. The electrical conductivity data are available in two distinct temperature domains, broadly corresponding to the glass and liquid regions. The inset graph focuses on the high temperature data. In the interval separating these two regions, no conductivity data for the liquid can be obtained because of partial crystallization. The kink in the electrical conductivity data is interpreted as the glass transition ( $T_g$ ), located at ~670°C for the three samples. The straight lines are polybaric regressions calculated with the Arrhenius laws (Table 3). For comparison, the conductivity law for a dry obsidian is shown (dashed line, Gaillard, 2004).

Figure 6 : Effect of pressure on the electrical conductivity in the glass (a) and the liquid (b) regions for the three samples. Only the data for the dry samples are shown. The straight lines are polybaric regressions calculated with the Arrhenius laws (Table 3). The effect of pressure is to decrease the electrical conductivity in both the glass and the liquid regions.

Figure 7 : Effect of water on the electrical conductivity. (a) Results for the phonolite composition sample from 1050 to 1300°C. (b) Variation of the electrical conductivity with the  $H_2O$  content of the liquid for the phonolite and the phonotephrite samples. The  $H_2O$  content corresponds to the initial  $H_2O$  concentration in the starting glass samples (Table 2). Data at 200 and 300 MPa.

Figure 8 : (a) Comparison at 1 atm between activation energies ( $E_a$ ) for ion mobility determined from electrical conductivity measurements (this study; Gaillard and Iacono Marziano, 2005; Scarlato et al., 2005 ; Gaillard, 2004; Park and Ducea, 2003 ; Tybureczy and Waff, 1983, 1985; Presnall, 1972) and Na diffusion experiments (Henderson, 1985; Jambon, 1982). Data for rhyolitic ( $NBO/T < 0.1$ ) to basaltic ( $0.7 < NBO/T < 0.8$ ) anhydrous melts. The straight line is the fit corresponding to our data, the dashed line fits the data of Tybureczy and Waff. (b) Compensation plot for the conductivity of silicate melts. Data from this work, dry and hydrous products and the studies mentioned above. The straight line is the fit corresponding to the whole data (see text).

Table 1 : Compositions of starting glasses.

Sample	VES9	VS88-65B	VES19
Eruption Rock type	VII-VIII century Tephrite	Pollena (472AD) Phonotephrite	Pompei (79AD) Phonolite
Phase	gl	gl	gl
SiO <sub>2</sub>	49.24	48.54	55.73
FeO <sub>total</sub>	7.20	5.79	1.95
Na <sub>2</sub> O	1.97	3.54	6.11
K <sub>2</sub> O	5.98	7.70	10.14
Al <sub>2</sub> O <sub>3</sub>	15.14	17.95	21.94
MgO	6.26	3.26	0.19
CaO	11.46	9.09	2.87
P <sub>2</sub> O <sub>5</sub>	0.94	0.46	0.07
F	0.14	-	0.37
TiO <sub>2</sub>	0.96	0.69	0.16
Cl	0.12	-	0.30
SO <sub>3</sub>	0.05	-	0.02
Total	99.48	97.27	99.85
NBO/T	0.73	0.46	0.11

Table 2: Description of experiments.

Sample	Apparatus	H <sub>2</sub> O (wt%) before exp.	H <sub>2</sub> O (wt%) after exp.	P (MPa)	T range (°C) <sup>3</sup>	Duration (h)
VES19	1 atm furnace	0	0	0.1	465-1256	7
VES19 <sup>2</sup>	IHPV	0	0	50	450-1301	4
VES19 <sup>2</sup>	IHPV	0	0	100	452-1300	4.5
VES19 <sup>2</sup>	IHPV	0	0	200	450-1301	4.25
VES19 <sup>2</sup>	IHPV	0	0	400	450-1304	3.5
VES19	IHPV	1.1 <sup>1</sup>	0.9 <sup>1</sup>	200	352-1276	7
VES19	IHPV	5.6 <sup>1</sup>	3.1 <sup>1</sup>	300	450-1250	7.5
VS88-65B	1 atm furnace	0	0	0.1	451-1323	28
VS88-65B <sup>2</sup>	IHPV	0	0	200	450-1325	6
VS88-65B <sup>2</sup>	IHPV	0	0	400	450-1300	9
VS88-65B	IHPV	3.5 <sup>1</sup>	2.0 <sup>1</sup>	200	455-1275	6.5
VES9	1 atm furnace	0	0	0.1	460-717	8.5
VES9	1 atm furnace	0	0	0.1	1205-1302	1
VES9 <sup>2</sup>	IHPV	0	0	50	448-1300	17.5
VES9 <sup>2</sup>	IHPV	0	0	200	448-1300	3.25
VES9 <sup>2</sup>	IHPV	0	0	400	449-1299	3.25

<sup>1</sup> Water contents determined by Karl Fischer Titration.

<sup>2</sup> Same sample.

<sup>3</sup> Includes the interval of crystallisation: ~[800; 930°C] for VES19, ~[850; 1200°C] for VS88-65B, ~[870; 1200°C] for VES9. Values within these intervals are not considered.

Table 3: Domains of validity and parameters of the Arrhenius laws<sup>1</sup>.

Sample	H <sub>2</sub> O (wt%)	P range (MPa)	T range (°C)	Ea (kJ/mol)	Lnσ <sub>0</sub> (ohm.m) <sup>-1</sup>	ΔV (cm <sup>3</sup> /mol)	Number of heating cycles
<i>Below T<sub>g</sub></i>							
VES19	0	0.1-400	450-671	81 (1)	7 (0)	18 (1)	5
VES19	1.1	200	352-500	86 (1)	7 (0)	18 (1) <sup>2</sup>	1
VES19	5.6	300	450-550	107 (6)	9 (1)	18 (1) <sup>2</sup>	1
VS88-65B	0	0.1-400	450-671	92 (4)	7 (1)	20 (2)	3
VS88-65B	3.5	200	455-630	129 (8)	13 (1)	20 (2) <sup>2</sup>	1
VES9	0	0.1-400	448-675	80 (3)	4 (0)	22 (2)	4
<i>Above T<sub>g</sub></i>							
VES19	0	0.1-400	700-1304	94 (1)	9 (0)	22 (2)	5
VES19	1.1	200	1050-1276	66 (1)	7 (0)	22 (2) <sup>2</sup>	1
VES19	5.6	300	1050-1250	61 (0)	7 (0)	22 (2) <sup>2</sup>	1
VS88-65B	0	0.1-400	675-1325	117 (2)	10 (0)	24 (3)	3
VS88-65B	3.5	200	1050-1275	105 (1)	10 (1)	24 (3) <sup>2</sup>	1
VES9	0	0.1-400	690-1301	142 (2)	12 (0)	16 (2)	4

<sup>1</sup>Lnσ = Ln σ<sub>0</sub> - (Ea+PΔV)/ RT.

<sup>2</sup>For hydrous samples, ΔV hydrous =ΔV dry.